# Synthesis of engineered particulates with tailored properties using dry particle coating

Robert Pfeffer *, Rajesh N. Dave, Dongguang Wei, Michelle Ramlakhan

*Particle Technology Center, New Jersey Institute of Technology, 210 YCEES Building, 161 Warren Street, Newark, NJ 07102-1982, USA*

## Abstract

Dry particle coating is used to create new-generation materials by combining different powders having different physical and chemical properties to form composites, which show new functionality or improve the characteristics of known materials. Materials with relatively large particle size (1–200 μm) form a core and these core (host) particles are mechanically coated with fine submicron (guest) particles; no liquid of any kind (solvents, binders or water) is required. A number of different devices used to achieve dry particle coating are reviewed. The fundamental mechanisms by which these devices achieve coating are discussed, and many examples of coated particles produced by these methods in our laboratory, as well as by other researchers, are described. Attempts to model some of these processes, so as to be able to predict suitable operating conditions and processing times for different host and guest particle properties, are also described. A theoretical predictive capability is necessary, not only to determine which of the devices would give the best results in a specific application, but also for scale-up and optimization. Based on our research, we believe that dry coating is a viable alternative to wet coating and can be used successfully for certain applications where wet coating processes are not feasible. © 2001 Elsevier Science B.V. All rights reserved.

## 1. Introduction

Particle coating to alter the surface properties and/or functionality of fine particles or powders is very important to many industries. Typically, surface modification of particles is done by wet coating methods such as pan coaters and a variety of fluidized bed coaters or by wet-chemistry based techniques such as coacervation, interfacial polymerization, and urea/formaldehyde deposition. However, wet coating methods have become less desirable recently because of environmental concerns over the resulting waste streams and possible VOC emissions. Dry coating, which directly attaches tiny, submicron-sized (guest or fine) particles onto relatively larger, micron-sized (host or core) particles without using any solvents, binders or even water, is a promising alternative approach.

Wet particle coating is used primarily to form a barrier or film between the host particle and its environment whose purpose is to produce extended or delayed release, separation of incompatibles, protection from water vapor, light or oxygen, taste masking, etc. Presently, most commercial coatings of particles, seeds, grains, granules or pellets are done using a wet process. For example, wet processes have been used in the pharmaceutical industry to coat solid dosage forms such as tablets, to create film coatings for controlled release of drugs, and for taste masking. They are used in the food industry for flavor enhancement, and for improving the appearance and stability, or shelf life, of a product, and in the agricultural industry for coating of seeds and for the sustained release of pesticides and fertilizers.

While these are some of the more conventional applications of particle coating, relatively new dry coating processes are now becoming available, for which many more new and exciting applications are possible [1–12]. In dry particle coating process, submicron-sized guest particles are coated onto larger, micron-sized host particles in order

* Corresponding author. Tel.: +1-973-642-7496; fax: +1-973-642-7496.
*E-mail address:* pfeffer@njit.edu (R. Pfeffer).

to create value-added composite particulate materials. In contrast to wet particle coating, the guest particles are brought into close contact with the host particles through the application of mechanical forces. Since the size of the guest particles are so small, van der Waals interactions are strong enough to keep them firmly attached to the host particles. Thus, either a discrete or continuous coating of guest particles can be achieved depending on a variety of operating conditions including processing time, weight fraction of guest to host particles and particle properties (see Fig. 1).

Continuous coating can consist of either a particle layer (monolayer or multilayer), which is porous, or a continuous film coating, which is generally non-porous. While continuous coatings are generally preferred, the ability to create discrete coatings has some unique advantages. For example, in some applications, a coating may be required to change a specific surface property, but a complete shielding of the underlying core particle is undesirable.

Sometimes, in addition to bringing the guest particles in close vicinity to the host particle, the process can either deform the guest particles or cause the guest particles to become embedded onto the surface of the host particle. The increased contact area due to deformation or embedding causes the attraction between the particles to become even larger, and a much stronger coating is obtained.

Apart from forming a barrier as in wet coating, dry particle coating can be used for making significant changes in the properties and/or the functionality of the original host particles, thus creating engineered particulates with tailored properties. Some examples of surface properties that can be improved or modified are flowability, dispersibility, solubility, wettability (hydrophilic/hydrophobic properties), electrostatic, electric, magnetic, optical, color, flavor, taste, particle shape/sphericity, sinterability, and solid phase reactivity. This opens up many new avenues of research and applications. For example, if one could change the sinterability of particles through coating them to decrease their sintering temperature (activated sintering), better ceramics and powder metallurgy products can be manufactured. On the other hand, by increasing the sintering temperature of the powder (deactivated sintering), one can create particulates that can withstand higher temperatures before their surface softens, agglomerate and fuse together, thus allowing certain processes such as catalytic fluidized bed reactors to operate at higher temperatures. This interesting new application of dry particle coating is described later on in this paper in more detail.

In addition to producing materials with completely different functionality, dry coating processes have an advantage of being cost effective due to the reduced use of high-priced or rare materials since the more expensive material (guest) can be coated onto the cheaper carrier material (host). Another major advantage of dry particle coating processes is that they are environmentally benign, producing none of the organic (gas or liquid) or aqueous waste streams, which usually are present in wet coating processes. Moreover, they can result in substantial energy savings because there is no need for drying the particulate products obtained.

Dry particle coating processes, as opposed to wet coating processes, are relatively new. They were pioneered, mostly in Japan, about 10 to 15 years ago, and are still in the R&D stage of development and are rarely used commercially in the US. The objective of this paper is to provide both a historical background (review) of this interesting subject and to describe the research efforts by our own dry particle coating group at NJIT. It is hoped that this paper will not only increase the visibility of these processes but also inspire others to work in this field resulting in a better understanding of the physico-chemical principles that influence dry coating as well as lead to new industrial applications.

The paper is divided into the following sections: background and historical perspective on dry coating is presented in Section 2, major devices used for dry coating are described in Section 3, applications of these processes are described in Section 4, our research at NJIT is described in Section 5, and a brief summary is given in Section 6.



Fig. 1. Schematic of dry particle coating.

## 2. Background on dry particle coating

The subject of dry particle coating is very closely related to the subject of dry mixing of powders. Ideally, a binary mixing process should intimately mix the two species so that any small sample taken from the mixture
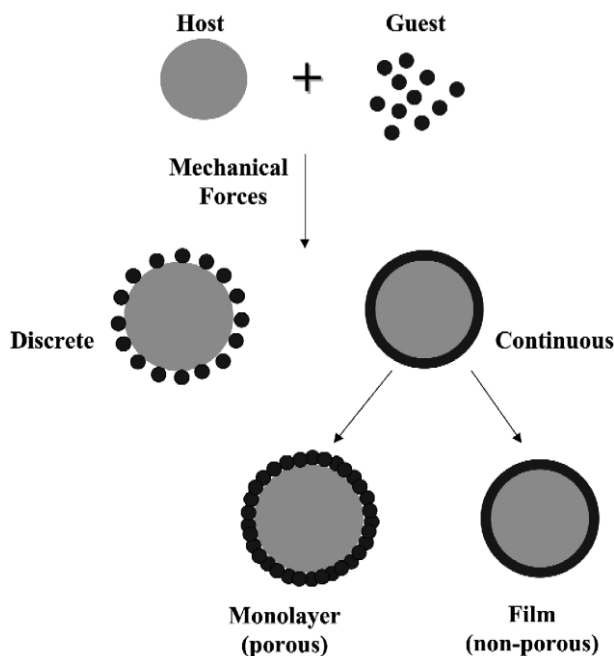
would contain the same proportion of the two constituents. This is hard to achieve, particularly when the powders are either cohesive, or the two species to be mixed are quite disparate in size. When the powders are cohesive they naturally form agglomerates and mixing two constituents requires breaking-up of the agglomerates. When the constituents differ in size there is an increased tendency for segregation as the size difference becomes larger. However, when the two components to be mixed are very different in size (one or two orders of magnitude), then segregation may no longer be a problem. In such cases, the smaller particles tend to adhere onto the larger particles. The adhesion force between the smaller particle and the larger particle is greater than the weight of the smaller particle, and hence it is not easily removed from the host. This phenomenon is usually referred to as "ordered mixing" or "structured mixing" and is shown schematically in Fig. 2.

In ordered mixing (a term coined by Hersey [13]), the surface of the larger particles (the first component of a binary mixture) is loosely coated/covered with smaller particles (the second component of a binary mixture). In dry particle coating, the same thing happens; however, the surface covering is more permanent because of a stronger physical (or chemical) bonding. Thus, ordered mixing and dry coating of powders are closely related, and therefore it is important to look at the literature on ordered mixing which precedes the literature on dry coating.

Initial work on ordered mixing was done by Hersey and co-workers [13–19], mainly for the purpose of pharmaceutical applications. Orr [20–22] coined the term "regimented" mix or "interactive" mix for this phenomenon. Staniforth and colleagues [23–28] also studied ordered mixtures applicable to the pharmaceutical industry. The main reason why this topic is so interesting to the pharmaceutical industry is that, in direct tableting, it is advantageous to have a microfine active ingredient attached to a coarse excipient. Besides eliminating the problem of segregation,
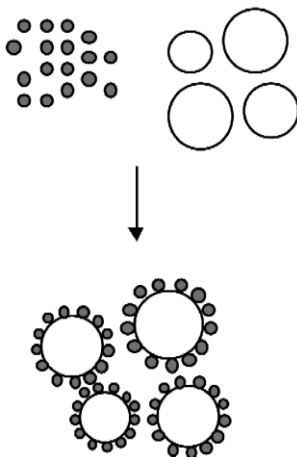
there are other advantages. The active microfine ingredient allows for higher dissolution rates, in some cases even making a hydrophobic drug soluble [29], and the coarse excipient gives the mixture better flowability and tableting properties.

The advantage of ordered mixing is that it provides a much better degree of homogeneity as long as the particle size distribution of the larger size species is not too wide [13,19,30,31]. Hence, in terms of subsequent segregation, ordered mixtures are more stable than ordinary mixtures [13,19,28,30,32–36]. It was also discussed in this literature that having a very wide size distribution of the large size species may lead to "ordered unit segregation" [16,37–40], which should be avoided.

While there is little available in terms of quantitative modeling of the ordered mixing process (except work by Alonso and co-workers, [41–44]), a qualitative explanation is given in Ref. [30]. Three stages are identified as: (1) separation of the agglomerates of the fine constituent into their primary particles, (2) bonding of these fines to the carrier particles, and (3) redistribution and exchange of fines among the carrier particles until a random distribution is achieved. While the real process may not take place exactly in that order, it is clear that the de-agglomeration of fines must occur in order to create such a mixture. Therefore, any mixing device, in order to achieve ordered mixing, must provide sufficient mechanical or other means of agitation to promote de-agglomeration of fines, i.e., provide a large number of particle collisions involving high normal and shear impact forces. Machines that can be used for this purpose are high intensity mixers and grinding machines such as ball and media mills.

There is another reason why ordered mixing and/or dry coating work well when using grinding type machines. It is easier to break up agglomerates into primary size particles in the presence of coarser particles in the mix when processed in a milling machine than having fine particle agglomerates alone. While this was only speculated in Ref. [18], later, Alonso [44] showed this through statistical computer simulations. This phenomenon works to the advantage of dry particle coating when performed in a milling type machine because the host particles act as the media and help in de-agglomerating the fines.

It is likely that the earliest dry coating work may have been done using some type of milling device by researchers involved with ordered mixing applications. However, the earliest reference to a device specifically used for dry coating comes from the Japanese literature, when it was discovered (by serendipity) that a new machine developed for ultrafine grinding [45] could also be used for dry particle coating [46]. The grinding device called the Angmill was used for creating particulate materials with different surface properties due to the strong mechanical force acting on the particles [46]. Since the combination of high shear and compression forces acting on the host and guest particles actually produced some surface fusion, the



Fig. 2. Ordered mixing.

treatment was termed mechanofusion, and the device, manufactured by Hosokawa Micron, is also called Mechanofusion®. A schematic of the mechanofusion device is shown in Fig. 3. Several articles were published during the 1980s describing the applications of mechanofusion [2,4,8,47]. Another excellent review paper on mechanofusion appeared later [1], and discussed the applicability of mechanofusion for powder surface modification from the perspective of comminution.

The concept of ordered mixing was also taken one step further (to dry coating) by using dry impact blending, as described in a series of papers by another Japanese group [48–51]. They argued that an ordinary dry blending process would result in an ordered mixture, as the fine particles attach to the larger host particles through electrostatic forces [51]. However, upon processing in an impact blending device, the large impulsive forces cause the fine particles to become firmly attached to the core particle and a coated composite particle is obtained. This device, called the Hybridizer®, is manufactured by Nara Machinery of Japan. The hybridizer, shown schematically in Fig. 4, has proven very useful for pharmaceutical applications; for example, it accelerated aspirin dissolution when coated onto an excipient such as potato starch [52].

The mechanofusion and hybridizer machines referred to above can produce chemical as well as physical surface interactions between the host and guest particles. While the latter deals with adhesion between the hosts and guests and de-agglomeration of the guests, the former deals with the change in the chemical or electronic states of the host and guest species as a result of the intimate mixing caused by the mechanical forces generated by the machines. If, in addition to physical adhesion, a chemical reaction occurs at the host–guest interface, the process is called mechanochemistry.

For example, a series of publications by Senna [53–56] has shown that dissimilar metallic species, notably complex oxide powders can be cross-linked by oxygen using a soft mechanochemical process (mechanical stressing of the
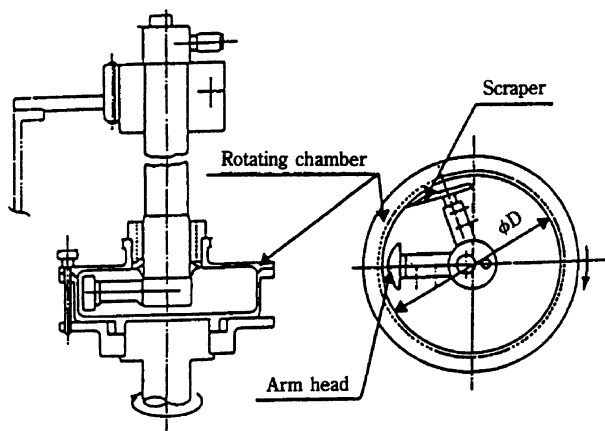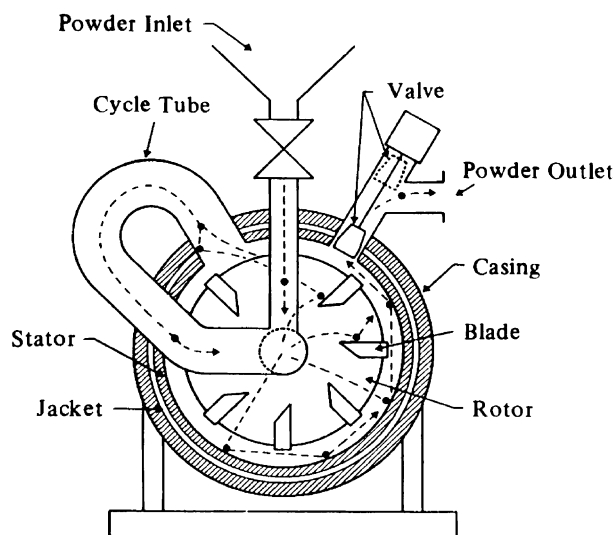


Fig. 4. Schematic of the hybridizer process.

powders) by proton transfer through OH groups, and subsequent electron transfer. The mechanochemical reaction is not restricted to inorganic materials, but is also applicable to complex formation between inorganic–organic or organic–organic materials and can be accomplished using easily available machines for grinding or comminution. Thus, mechanochemical effects are very important considerations in the understanding of dry particle coating processes. Specific examples of these effects (coating of silica onto cornstarch and cellulose) will be presented in Section 5.

Both the mechanofusion device and the hybridizer produce coated particles where the level of forces that the guest and host particles are subjected to is very high. In certain applications, these high forces are unnecessary or even detrimental to the final coated product obtained, for example, excessive size reduction of the host particles. Devices that produce "softer" coatings by applying a smaller level of forces have also been introduced. An elliptical rotor type powder mixer, called the Theta Composer® (see Fig. 5), was developed for this purpose and manufactured by the Tokuju Company in Japan. Several articles describe the operation of the theta composer, which has been found to be very useful for processing (coating) certain pharmaceutical and food products [44,57–60].

Another "softer" dry coating method uses a magnetic field to accelerate and spin larger magnetic particles mixed in with the core and guest particles promoting collisions between the particles and with the walls of the device. This magnetically assisted impaction coating (MAIC) process [61,62] developed by a US company, Aveka, results in very good mixing and produces mechanical stresses sufficiently large to promote adherent coating of the guest particles onto the surface of the core particles. A schematic of the MAIC is shown in Fig. 6. In our own laboratory [9,11], we have successfully used the MAIC process for a
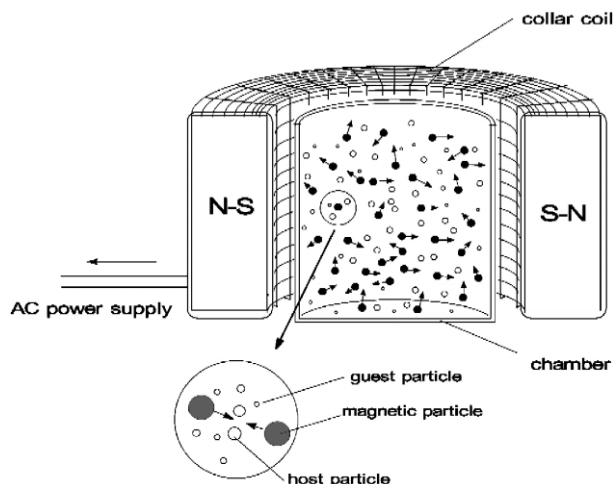


Fig. 3. Schematic of the mechanofusion process.

Fig. 5. Schematic of the MAIC process.



bubbles

Fig. 7. Bubbling occurs when operating the bed above minimum fluidization conditions.

number of different applications, including the coating of silica onto cornstarch. These applications will be fully described in Section 5.

While most of the literature in dry coating comes from Japan, during the last few years, several concentrated activities in this area (some proprietary, and not yet described in the literature) have been initiated in the US. At NJIT, a new device was invented within our group, based on the principle of centrifugal fluidization (Fig. 7). This device called the rotating fluidized bed coater (RFBC) [12] can also produce soft coatings. More details of this device are provided in the next section.

Most recently, a novel class of coating technique has been proposed based on the concept of direct fine particle generation and subsequent coating onto host particles. In one such process, nano-sized guest particles are generated by laser ablation of a target (e.g., Ag, $Y_2O_3:Eu^{+3}$, and $TaSi_2$), and the particle flux in a plasma is directed towards a small fluidized (caused by vibration) bed of micron-sized host particles [63–65]. While difficult to
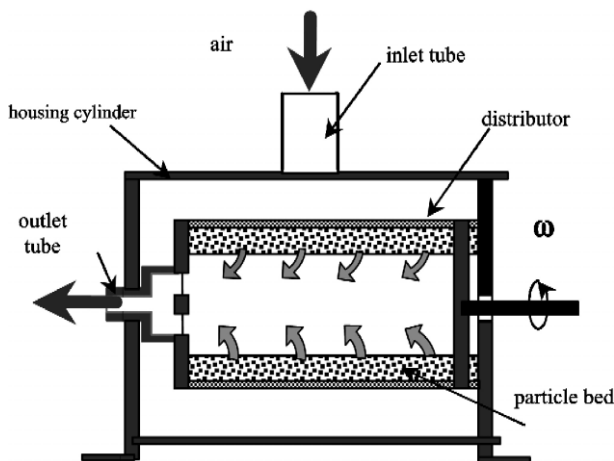

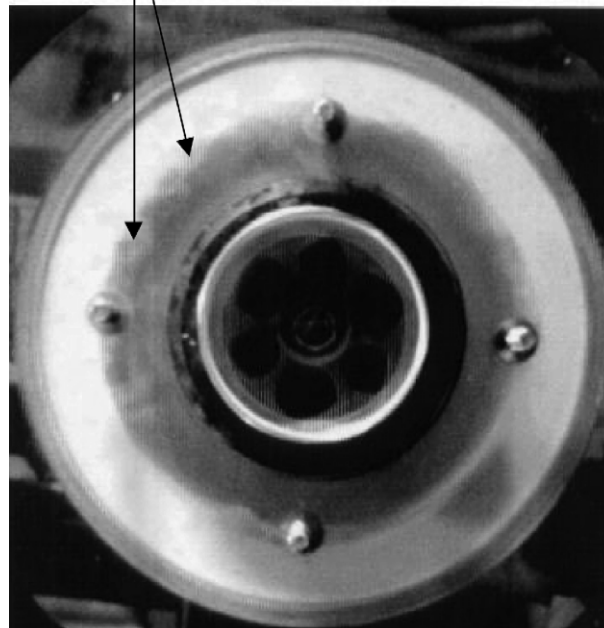
Fig. 6. Schematic of the rotating fluidized bed coater.

scale-up, this laser ablation technique can coat very fine (less than 5-$\mu$m host particles) by ultrafine guest particles, an important consideration for the pharmaceutical industry. Similar processes based on sputtering and other techniques that allow for producing a flux of nano-particles have also been proposed.

The operating principles of each of the coating devices referred to above are different; hence, the type of coating produced and the applications for which they are optimum are also different. Coatings can be characterized into several categories such as deep embedding, encapsulation, filming, discrete or partial surface covering, and a loose surface coating (ordered mixture). Although all of these types of composites can be obtained by using one of the available dry coating devices, there is a lack of understanding of the underlying physico-chemical principles that govern the coating process. Such an understanding is necessary to predict the choice of machines and the right combination of process variables needed to produce composite materials with desired tailored properties.

The current state-of-the-art approach is to use a trial and error procedure to determine whether the process works or not. This approach is clearly inadequate, not only because it is very time consuming, but also because it does not allow determining the conditions for obtaining the optimal quality. However, to date, very little work has been done to develop macroscopic models for these processes because the modeling of these processes is not straightfor-

ward and different devices employ different mechanical mechanisms to achieve coating.

The modeling work reported in the literature is mostly based on the earlier work on ordered mixing. Based on experimental observations and the concepts of statistical modeling, Alonso [41] explained the basic mechanisms of dry coating. He argued that initially the coating consists of loose agglomerates of fines adhering to the host particles in their immediate vicinity. This occurs rather quickly and is followed by the dispersion and rearrangement of fines spread over the surface due to collisions between a coated host and a non-coated host. This process is viewed as a second-order reaction between coated (C) and non-coated (N) particles: $C + N \rightarrow {}^{k} C + C$.

For the mechanofusion device, a qualitative picture of the process was proposed to provide a relationship between the measured BET surface area of the composites and the specific energy consumption of the device [1]. Again, the process was described in two steps, adhesion of the guest particles onto the host particles' surface and then compaction of the guest particles. A preliminary model for mechanofusion (see next section for a detailed description of the device) has been proposed by considering the particles as a continuum and introducing an inner piece action zone [66]. In this analysis, the effect of the scraper has been neglected. The model predicts that the force acting on the particles is proportional to the square of the angular speed, and increases with a decrease in gap distance. These results qualitatively agree with some experimental measurements. While the analysis does not take into account the material properties, it can provide rough guidelines for the powder loading in the chamber and the selection of rotational speed.

An analysis of the coating process in the hybridizer was carried out by statistical simulations to compute the energy of adhesion for formation of a monolayer under the assumption that Coulomb and London–van der Waals interactions work together [51,67]. This allowed for predicting the (qualitative) effect of two important factors of the coating process, namely, the size of the particles, and the size ratio between host and guest.

The ability to improve the flowability of a material by coating with fine particles has been discussed by Mei et al. [68]. The authors used a discrete element simulation of powder flows between a moving and a stationary plate to examine the effect of fine coatings on the surface of a larger substrate. They also developed an extended Johnson–Kendall–Roberts (JKR) particle contact model to include the effect of particle coating on the force–displacement relationship due to surface energy and elastic deformation. Their results indicated that the cohesion force between two primary particles in the presence of a fine coating is directly proportional to the size ratio of the coating particles to the host powder particle and results in drastic reduction in the cohesion forces. This argument has been adapted to explain the improved flowability of corn-

starch and cellulose in the presence of a discrete coating of silica after processing in the MAIC device (see Section 5). The fine silica particles reduce the Van der Waals attraction force between the host particles making them flow more easily. The number of guest particles on the surface of the host particles have only a minor effect on the flowability once the cohesion force is reduced by one or more coating particles. Hence, even with a very discrete coating on the surface of the host particle, there is significant improvement in the flowability of the material.

Recently, within our group at NJIT [10,69] and elsewhere [70], discrete element modeling (DEM) simulations have been utilized to understand the particle motion in some of the coating devices. For the theta composer [70], it was found that the forces arising from particle–rotor interactions play a significant role. In addition, the rotor speed and more importantly the cohesive property of the particles, were important factors. Our DEM results are described in Section 5. We note that while the computational requirements for realistic simulations are still beyond the scope of present computers, the use of DEM, even with a limited number of particles, can provide significant insight into a particular coating process. Unfortunately, it is impossible to simulate a system with both host and guest particles present, hence the results from the DEM simulations need to be combined with statistical methods to develop a complete picture. This is a challenging area for further research.

## 3. Dry coating devices

As already discussed in the previous section, there are numerous devices available for dry particle coating. These devices, although different in their manner of supplying the necessary mechanical forces, all strive to efficiently promote the de-agglomeration of the guest particles and their adhesion onto the surface of the host particles. In the hybridizer the ultra high rotation of the blades and recirculation of the powder allows the host and guest particles to violently collide with each other. In mechanofusion, the particles are also subjected to severe shear and compressive stresses as they travel between the clearance of the rotating drum and the inner piece. In MAIC, magnetic particles spin furiously due to an oscillating electromagnetic field causing collisions between the host and guest particles and the walls of the device. In the theta composer, the guest particles are impacted onto the host particles by the high-speed motion of an elliptical rotor in an elliptical mixer. In the RFBC, de-agglomeration and impaction of the guest particles onto the hosts occur because the bed is fluidized at very high gas velocities resulting in very good mixing and high shearing stresses. All of these devices have been used successfully by many investigators to produce composite particles with unique and improved functionality, and, with the exception of the theta com-

poser, all are available at NJIT. In this section, we will describe these devices in some detail.

### 3.1. Mechanofusion

A schematic of the mechanofusion machine is shown in Fig. 3. The device consists mainly of a rotating outer vessel, a stationary inner piece and a stationary scraper. A measured amount of host and guest particles is placed into the rotating vessel. As the vessel rotates at speeds between 200 and 1600 rpm, the powder is forced outward towards the walls of the vessel. The gap between the inner piece and the rotating drum is controlled, and as a result, the particles passing through the gap are subjected to intense shearing and compressive forces. These forces generate sufficient heat energy to "fuse" the guest particles onto the surface of the host particles. The gap size between the inner piece and the walls of the vessel is very important in controlling the thickness of the desired coating. The gap between the scraper and the wall of the vessel is also controlled. The scraper breaks up and disrupts any build-up or caking of the particles on the walls of the vessel. This is a batch-operated device.

There are several advantages in using the mechanofusion system. First, the shape of the inner piece, the small gap, and the high rotation speed of the drum allow the particles to be subjected to very high shear and compressive forces. Second, there is a local temperature build-up due to these strong forces acting on the particles, which can result in the fusion of the surface of the host and guest particles. This produces very strong physical and/or chemical bonds, which enhance the coating process.

### 3.2. Hybridizer

The hybridizer, shown schematically in Fig. 4, consists of a very high-speed rotating rotor with six blades, a stator and a powder recirculation circuit. The powder (host and guest particles) placed in the processing part of the vessel is subjected to high impaction and dispersion due to the high rotating speed of the rotor. The particles undergo many collisions, and this allows for break-up of fine agglomerates and powder coating due to the embedding or filming of the guest particles onto the surface of the host particles. Currently, this is a batch-operated device.

The hybridizer has several advantages that make it a powerful dry coating device. First, the rotor of the hybridizer can rotate anywhere from 5000 to 16,000 rpm. Due to the strong forces applied to the materials at these high rpm, very short processing times are required to achieve coating. Second, the device consists of a recirculating unit that continuously moves the particles in and out of the processing vessel and against the blades of the rotor. Lastly, similar to mechanofusion, there is a temperature build-up due to the high impaction forces caused by the high rotation speeds, which aids in coating the guest particles onto the surface of the host particles.

### 3.3. Magnetically assisted impaction coater (MAIC)

A schematic of the magnetically assisted impaction coating device is shown in Fig. 5. Although MAIC can be used in a continuous mode [71], the small bench-scale device used at NJIT operates in a batch mode. A measured mass of both host and guest particles are placed into a processing vessel (200-ml glass bottle). A measured amount of magnetic particles is also placed in the processing vessel. The magnetic particles are made of barium ferrite and coated with polyurethane to help prevent contamination of the coated particles. An external oscillating magnetic field is created using a series of electromagnets surrounding the processing vessel. When a magnetic field is created, the magnetic particles are excited and move furiously inside the vessel resembling a gas-fluidized bed system, but without the flowing gas. These agitated magnetic particles then impart energy to the host and guest particles, causing collisions and allowing coating to be achieved by means of impaction or peening of the guest particles onto the host particles.

There are several unique features of MAIC that makes it advantageous as a dry particle coating device. Firstly, the MAIC can coat soft organic host and guest particles without causing major changes in the material shape and size [11]. Secondly, although there is some heat generated on a microscopic level due to the collisions of particles, there is negligible heat generation on a macroscopic level and hence no increase in temperature of the material during processing by MAIC. This is desirable when processing temperature sensitive powders such as pharmaceuticals. Lastly, the device can be operated both as a batch and continuous system making it versatile in the amount of material it can process.

### 3.4. Rotating fluidized bed coater (RFBC)

This newly developed coating device operates on the principle of a rotating fluidized bed. The host and guest powder mixture are placed into the rotating bed and is fluidized by the radial flow of gas through the porous wall of the cylindrical distributor, as seen in Fig. 6. Due to the high rotating speeds, very high centrifugal and shear forces are developed within the fluidized gas–powder system leading to the break-up of the agglomerates of the guest particles. Moreover, the very large flow of air needed to fluidize the particles at high rotating speeds and the motion of bubbles when operating the bed above minimum fluidization conditions (see Fig. 7) creates strong mixing and hence good coating is achieved. For example, at "100 g's", the minimum fluidization velocity can be 2 orders of magnitude greater than in a conventional "1 g" fluidized
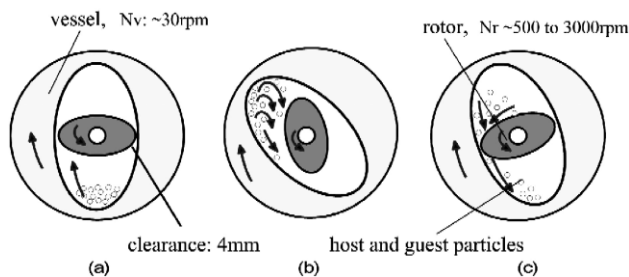
Fig. 8. Schematic of the theta composer: (a), (b) and (c) represent different orientations.

bed. The RFBC has another advantage over a conventional fluidized bed in that very small host and guest particles belonging to Geldart group C can be easily fluidized by increasing the rotating speed [72]. The RFBC also has the capability of being operated in a continuous mode.

*3.5. Theta composer*

A schematic showing the dimensions of the theta composer is shown in Fig. 8. The theta composer consists of a slow rotating elliptical vessel (around 30 rpm) and a faster (500–3000 rpm) elliptical rotor. As the rotor rotates inside the vessel, the powder mixture consisting of host and guest particles is subjected to shear and compressive stresses as it is forced into the small clearance between the vessel and the rotor. As the rotor continues to move and the clearance between the vessel wall and the rotor becomes large, there is bulk mixing of the host and guest particles, as shown in Fig. 8.

## 4. Applications of dry particle coating

Dry particle coating is applicable to a variety of industrially important problems. This is due to its ability to create engineered particulates with substantial improvements of certain physical and/or chemical properties. Early work from the Japanese literature report several interesting applications. For example, 5 $\mu$m polymethylmethacrylate (PMMA) particles coated with 10% by weight of 0.015-$\mu$m $TiO_2$ particles, using mechanofusion, flowed freely and had a near zero angle of repose. In contrast, both the original PMMA and $TiO_2$ particles did not flow well and had an angle of repose greater than 30° [4]. It was also reported that processing of ground polystyrene resin of 10-$\mu$m size with carbon black in mechanofusion produced easily flowing toner material of rounded shape [4]. The mechanofusion system is also capable of promoting a high level of de-agglomeration, as evidenced by processing 10-$\mu$m-sized agglomerates of polytetrafluoroethylene (PTFE), where each individual PTFE particle had a size of about 0.1 $\mu$m, with 5-$\mu$m spherical PMMA host particles. When examined using SEM, the composite particles showed an even coating of individual PTFE particles over the surface of the PMMA particles indicating that the PTFE agglomerates were broken up and well dispersed. Mechanofusion processing also resulted in a significant increase in negative polarity of PMMA particles [4] in contrast to the uncoated PMMA, which was electrically neutral.

Most of the early work reported using the hybridizer involved processing of pharmaceutical drugs to produce controlled-release properties [52,73,74]. As an example, fines of isoproterenol HCl, 5% by mass, were coated onto potato starch ($\sim 70$ $\mu$m) followed by a coating of carnauba wax, 5% by mass, to achieve time-released control of isoproterenol HCl. Furthermore, it has been reported that the hybridizer was useful in preparing composite and encapsulated (film-coated) particles. For instance, if inorganic fine particles were used as coating materials, they were fixed and embedded in the surface of core particles, and if polymer or metallic fine particles were used as coating materials, they partially melted and produced a continuous film coating on the core particle [67].

Many other applications of dry coated composite materials can be found in the literature (see a survey in Ref. [1]) such as coloring and UV protection in cosmetics, production of toner particles with different colors, metal/ceramic composites, thermal spray materials, ceramic filters, solid lubricants, and electric contact materials. Other applications using mechanofusion and the hybridizer include production of yttrium-based superconductors [75]; production of nanocrystalline thin films of metal oxides such as $TiO_2$ and $SnO_2$ with a highly porous structure for use in photoelectrochemical cells [76]; production of copper matrix molybdenum particle composites by hot pressing copper coated molybdenum powder to achieve improved properties such as low porosity, high hardness, and a lower coefficient of thermal expansion [77]; coating of silicon nitride particles with an alumina precursor to make $Si_3N_4$ behave like $Al_2O_3$ in aqueous slurries and to achieve high packing density [78,79]; improvement in properties of artificial bone material hydroxyapatite (HAP) by coating with partially stabilized zirconia to provide high fracture toughness while preserving the original surface properties of HAP [80]; and improving the performance of liquid chromatography (HPLC) by using uniform polyethylene microspheres coated with silica [81]. In addition, using the theta composer, softer coatings for controlled release microcapsules [58] and food materials containing cellulose fibers [59] were produced. More details of this latter application are given in Section 5.

There are also some novel applications of dry coating not yet reported in the literature. For example, the coating of titania onto tiny glass bubbles using a dry coating process can be used for cleanup of oil spills. The glass bubbles will float over the oil spill, and titania, being photo-active, will react with the oil and decompose it. The glass bubbles will eventually end up on the shore as part of

the sand. Fine particles of titania are very difficult to handle in such an application by themselves, but using larger hollow glass particles as carriers makes them not only floatable, but easy to handle. Another interesting example is coating nitrogen-fixing bacteria onto grass seeds. The coated seeds can provide their own fertilizer when planted in the soil. These two examples are quite different from the traditional "barrier type film coating" applications. Similarly, a novel application, requiring discrete coating as compared to film type coating, developed by our own group for "deactivated sintering" is described in Section 5.

In addition to coating, it was found that these machines could also be used for other types of powder processing such as rounding of particles and precisely mixing different kinds of powders together. For example, the Hosokawa mechanofusion machine has been successfully used for mixing powder materials for superconductive oxides, multi-component targets for thin films and electric wires of Bi-based superconductive oxides [82–84]. The diverse examples described above indicate the huge potential market that exists for developing new particle composites for applications in foods, consumer products, cosmetics, pharmaceuticals, biomaterials, inks and toners, and ceramics.

# 5. NJIT research in dry particle coating

Our research is concentrated on the study of MAIC, mechanofusion, the hybridizer, and the RFBC. The fundamental objectives are to create new engineered particles, to study the mechanisms of coating in each device both experimentally and theoretically (through DEM simulations), and to compare the coating performance of these devices. The following sections outline some of our accomplishments and contributions to dry particle coating.

## 5.1. Experimental studies

Each coating device was individually studied by examining its coating performance. Several methods of surface coating characterization were utilized. A scanning electron microscope (SEM) was used to study the surface morphology and particle shape after coating. Energy dispersive X-ray spectroscopy (EDX) was used to study the surface composition of the coated products. The flowability of the products was analyzed by measuring the angle of repose (AOR) using a fixed base method. Wettability tests were conducted by using a penetration rate method to evaluate the hydrophilicity of the coated products. BET testing was used to measure surface area of particles. The robustness of coating was measured by placing the coated particles in an ultrasonic bath for different time periods. Particle size distribution was measured using an API Aerosizer and the mean particle size used throughout this paper is a volume-mean.

### 5.1.1. Surface modification to improve flowability and reduce wettability

MAIC was used to coat cornstarch (ARGO) and a microcrystalline cellulose powder (Avicel, PH200) with 1% silica to simultaneously improve the flowability and decrease the wettability of these powders. Cornstarch ($\sim 15$ $\mu$m) is frequently used as a food-thickening agent and as an inactive component of pharmaceuticals [85]. Microcrystalline cellulose (aspect ratio of 4:5, $\sim 180/40$ $\mu$m) is one of the most important pharmaceutical excipients used in tableting, especially for direct compression and is also used as a food additive to bring fiber into the diet. However, their cohesiveness (especially cornstarch) can create problems during handling and storage. Also, their hydrophilicity can reduce shelf life due to premature biodegradation and loss of mechanical properties due to plastization [86]. Only 1% by mass of silica (primary particle $\sim 0.3$ $\mu$m) was used to coat the particles to conform to the Food and Drug Administration (US FDA) standards; therefore, only very discrete coatings were obtained.

SEM images of uncoated and coated cornstarch are shown in Fig. 9(a) and (b), respectively. The coated sample shown was processed for 10 min. A very discrete coating was observed on the surface of the cornstarch particles (see Fig. 9(b)). The elemental mapping of silicon on the surface of the coated product is shown in Fig. 9(c) and confirms the presence of silica. The surface morphology of uncoated cellulose is shown in Fig. 10(a). The particles are fibrous and have an aspect ratio of 4:5. SEM images for cellulose host particles coated with silica guest particles for processing times of 5 and 10 min are shown in Fig. 10(b) and (c), respectively. Again, a discrete coating of silica is observed on the surface of both the 5- and 10-min processed samples, with an increase in surface coverage occurring with an increase in processing times.

Angle-of-repose (AOR) measurements were used to evaluate the flowability of the cellulose and the cornstarch products. The results are shown in Figs. 11 and 12, for cornstarch and cellulose, respectively. In Fig. 11 for cornstarch, there was a decrease in the AOR as a function processing time, indicating an increase in flowability with increasing surface coverage. In Fig. 12 for cellulose, there was a decrease in the AOR for 5- and 10-min processing time, but then an increase in AOR was observed for a processing time of 20 min. Further investigation of the coated cellulose products indicated a size reduction or breakage of the fibers at higher processing times. The increased surface area due to fiber breakage acts to decrease the flowability, so that the net effect (more coating but smaller particles) resulted in poorer flowing material at 20 min of processing time.
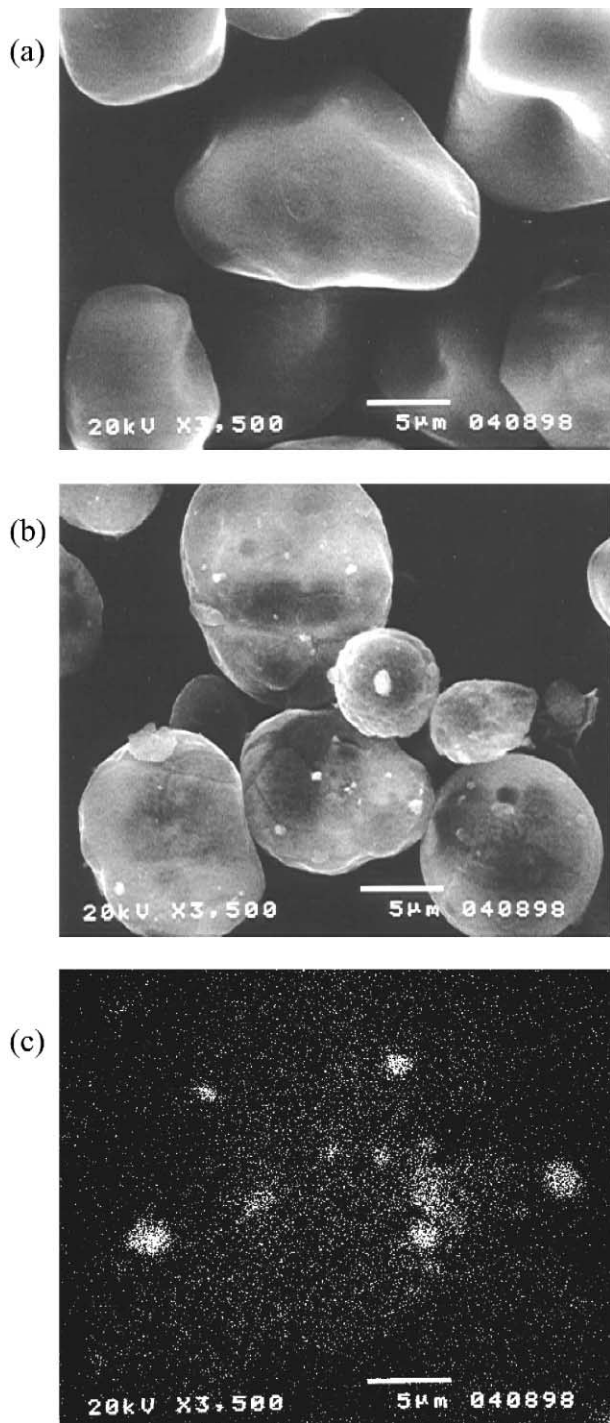
Fig. 9. SEM micrographs of (a) unmodified cornstarch, (b) cornstarch processed for 5 min and (c) EDX mapping of silicon on the surface of modified cornstarch.

sorbed 110% of its weight in water after an exposure time of 5 min. Uncoated cornstarch, also hydrophilic absorbed 60% of its weight in water. For cornstarch processed for 5 and 20 min, the amount of water absorbed was only 28% and 18% of their weight, respectively.

Water absorption capacities of unmodified cellulose and coated products at 5-, 10-, and 20-min processing times are shown in Fig. 14. The water absorbed for all processing times were lower than that of the unmodified cellulose
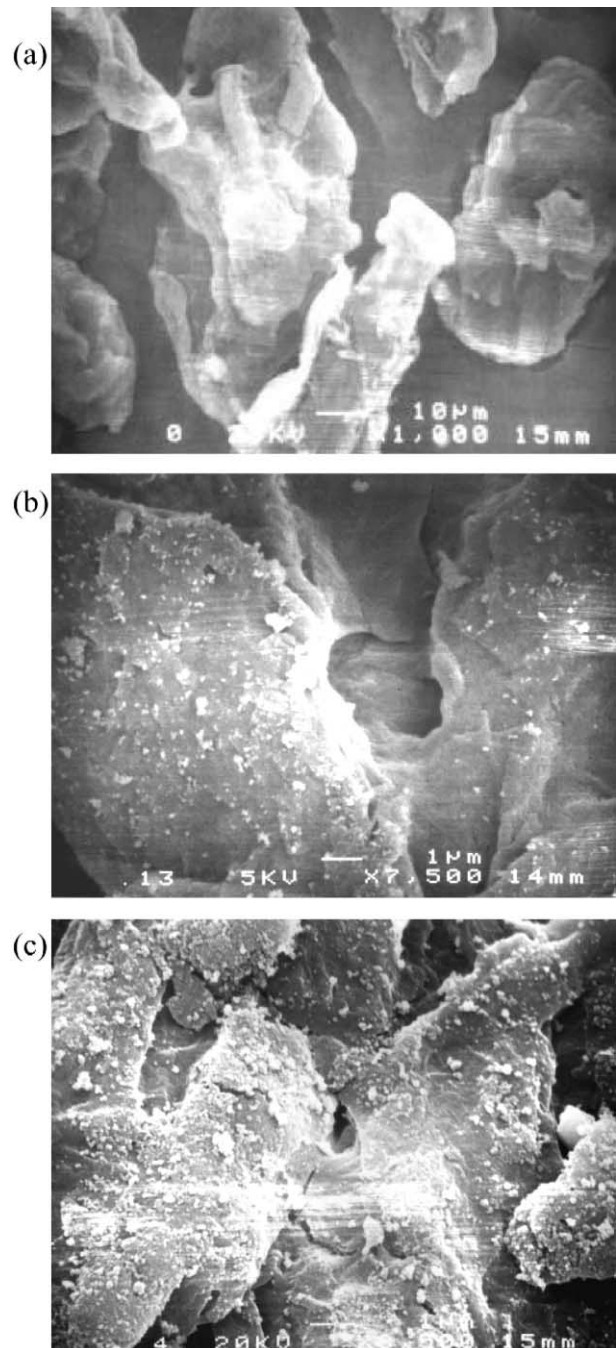


Fig. 10. SEM micrographs of (a) unmodified cellulose, (b) cellulose coated with silica for 5 min and (c) cellulose coated with silica for 10 min.

To measure changes in the hydrophilicity of the surface of cornstarch and cellulose, wettability tests were conducted. The method of testing selected was the rate penetration method [87,88]. The water absorption results for uncoated cornstarch, 5- and 20-min coated cornstarch, and silica only, for an exposure time of 5 min, are shown in Fig. 13. The fumed silica, being very hydrophilic, ab-

Fig. 11. Flowability of cornstarch as a function of processing time.

Fig. 13. Wettability study of (a) silica, (b) uncoated cornstarch, and cornstarch processed for (c) 5 min and (d) 20 min.

particles. Similar to the flowability result, the water absorption capacity after 20 min of processing was higher than after 10 min, again indicating attrition of the host particles with increased processing time.

The reduction in hydrophilicity is believed to result from the reaction of the acidic silanol groups $(-Si(OH)-)$ on the silica surface and the almost neutral hydroxyl groups $(-(OH)-)$ groups on the cornstarch/cellulose surfaces, to form hydrophobic $(-O-)$ groups (see Fig. 15) by releasing water molecules. The soft mechanical forces arising from the particle collisions during "fluidization" in MAIC promotes the reaction by mechanochemistry [89]. In order to confirm the hypothesis of a mechanochemical mechanism for the reduction in water absorption as described above, Fourier Transform Infrared Spectroscopy (FTIR) was used to measure the changes in OH groups before and after coating. FTIR results are presented in Figs. 16 and 17, for cornstarch and cellulose, respectively. In Fig. 16, there is a reduction in the absorbance caused by O–H stretching vibrations between the wavenumber of 3100 and 3650 cm$^{-1}$ for the coated samples as compared to the uncoated cornstarch, indicating a reduction in the O–H groups on the surface of the samples. There is also a significant reduction in absorbance due to O–H stretching vibrations with an increase in processing time from 10 to 20 min, again within the above mentioned wavenumber range.
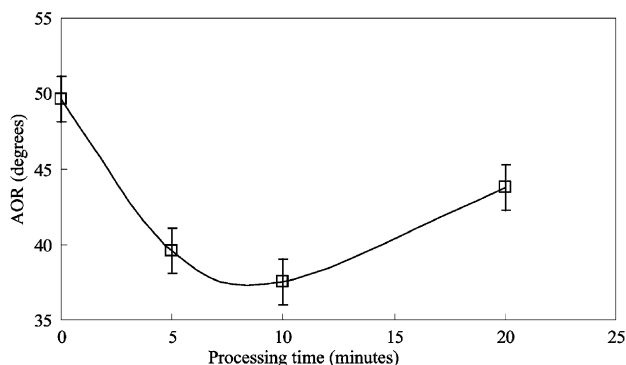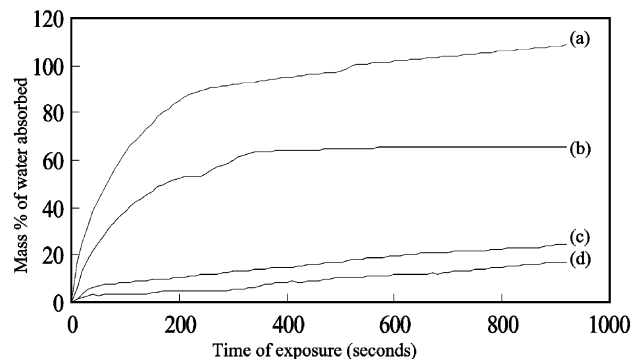
Fig. 17 (for cellulose) shows that the least absorption caused by O–H stretching vibrations is obtained for the 10-min processed sample. This appears to confirm the hydrophilicity results for cellulose presented in Fig. 14. The increase in absorption of the 20-min coated sample can be attributed to the significant reduction in the particle size of the cellulose fibers, making more O–H sites available for absorption due to increased surface area. The FTIR results lend proof to the hypothesis that MAIC processing caused a mechanochemical surface reaction between the corn starch/cellulose host particles and the silica guest particles.

The theta composer [59] was also used (by a research group in Japan) to simultaneously improve the flow and reduce the hydrophilicity of cellulose fibers. Results similar to our study using MAIC were obtained. The flowability of cellulose coated with 1% silica as a function of time is shown in Fig. 18. As the processing times increased to 8 min, so did the flowability of the product, as evident by a reduction in the AOR. After 8 min, there was a decrease in the flowability of the coated product. This was attributed to the reduction in the size of products due to the breakage of the fibers, with an increase in processing time. A wettability analysis of the products obtained using the theta composer showed similar trends to those obtained by

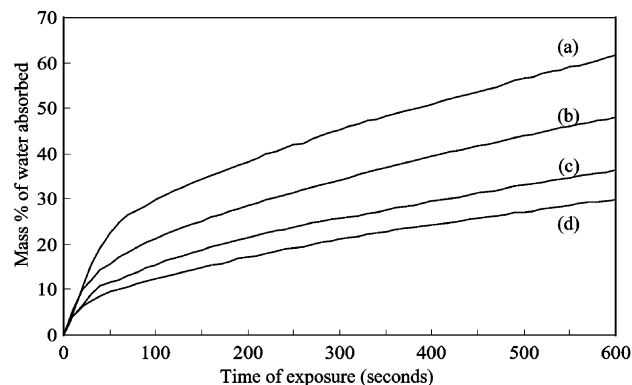Fig. 12. Flowability of cellulose as a function of processing time.

Fig. 14. Wettability study of (a) uncoated cellulose, and cellulose processed for (b) 20 min, (c) 5 min and (d) 10 min.
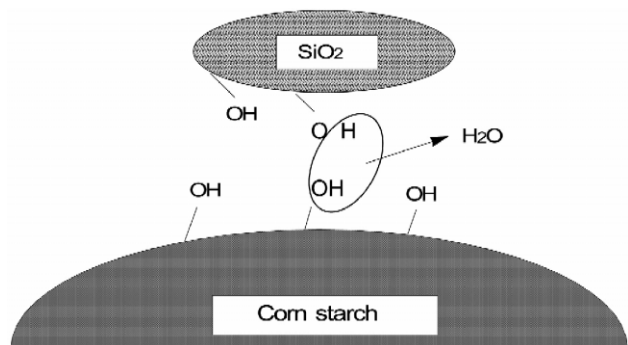
Fig. 15. Mechanochemistry effect occurring on the surface of cornstarch to form hydrophobic groups.

MAIC. The water absorption of the compressed products was measured as a function of exposure time. Again, it was found that there was a reduction in water absorption with increased processing times, but for the 10-min coated sample there was an increase (see Fig. 19).

### 5.1.2. Optimization studies of the MAIC

There are several critical system and operating parameters affecting the coating performance of the MAIC device. The system parameters are magnetic particle size and magnetic particle to powder (host and guest particles) mass ratio, and the major operating parameters are frequency, current (or voltage), and processing time. To study the effects of these parameters on the coating efficiency, a model system consisting of 200-$\mu$m spherical PMMA host particles and several sizes of alumina guests particles was chosen and experiments were conducted which systematically varied all of the parameters mentioned above.

The processing times investigated were 1, 3, 5, 7 and 10 min, respectively. The size of the alumina guest particles used was 0.2 $\mu$m. The mass percentages of alumina guest particles used were based on the assumption of 100% surface coverage of the host particles with a monolayer of guest particles. An increase in processing time from 1 to 5 min showed a corresponding increase in the percentage of surface area covered (see Fig. 20). SEM micrographs were quantitatively analyzed by a statistical technique by individually counting the number of guest particles on the surface of the host particles to obtain the percentage of surface covered. After 5 min, the amount of surface coverage achieved fluctuated slightly due either to small differences between detachment and reattachment of guest particles, after "an equilibrium" is reached or to experimental error, which is estimated at about 5%.

The effect of current on the coating efficiency was examined by varying the current at a fixed frequency of 45 Hz. The current was varied from 1 to 5 A. Each experiment was conducted for a processing time of 5 min, with a guest particle size of 0.2 $\mu$m. Using an optimum current of 5.0 A and a processing time of 5 min, the frequency of the system was varied from 45 to 100 Hz. An unusual behavior was observed. At 45 Hz, the surface coverage obtained was about 66%, then from 45 to 70 Hz, the surface coverage decreased with increasing frequency. After 70 Hz, the surface coverage of the coated product increased gradually with increasing frequency, where it again peaked in surface coverage at a frequency of 90 Hz. This behavior suggests that the variations in the frequency cause a periodic fluctuating behavior in the amount of surface coverage obtained.

The motion of the magnetic particles is responsible for the coating of guest particles onto the host particles by a vigorous "fluidized" type motion causing collisions between host particles and between host and guest particles. Therefore, the mass of magnetic particles used in the system significantly affects the surface coverage obtained. The magnetic particle to powder mass ratio was varied to determine the optimum mass of magnetic particle needed. Several ratios were investigated and it was found that as the magnetic particle to powder mass ratio increased, the
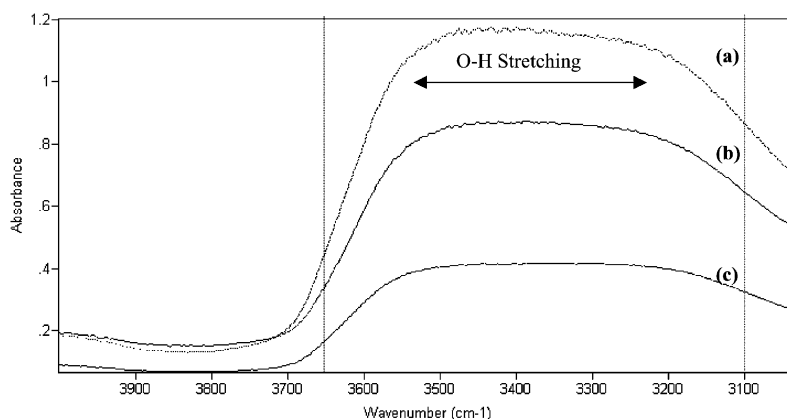


Fig. 16. IR absorption caused by O−H stretching vibrations for (a) uncoated cornstarch, (b) cornstarch coated for 10 min and (c) cornstarch coated for 20 min.
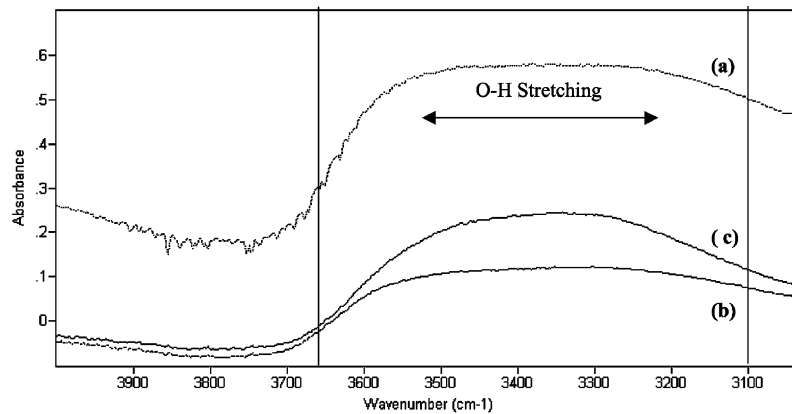
Fig. 17. IR absorption caused by O−H stretching vibrations for (a) uncoated cellulose, (b) cellulose coated for 10 min and (c) cellulose coated for 20 min.

percentage of surface area covered also increased. For ratios larger than 2, it has been shown that there is not much change in the coating efficiency, and in some cases coating is even poorer than at lower ratios [9].

The size effect of the guest particles on the coating efficiency was investigated using four sizes (provided by the manufacturer) of alumina guest particles: 0.05, 0.2, 0.4, and 1 μm. Based on complete coverage with a monolayer of alumina particles, the percentage of alumina by weight for each of these four sizes was chosen as 0.25, 1.0, 2.0, and 5.0, respectively. As the guest particles size increased, the area of coverage decreased as shown in Fig. 21. The two smallest sizes gave the best coating results. However, careful examination of the surface morphology of the products coated with 0.05- and 0.2-μm alumina showed that the PMMA particles coated with 0.2-μm alumina were more uniformly coated than the PMMA particles coated with 0.05-μm alumina [11]. Many more agglomerates of alumina were observed on the surface of PMMA for a guest size of 0.05 μm. This is probably due to the inability of the MAIC device to efficiently de-agglomerate the 0.05-μm size guest particles.

Three sizes of magnetic particles were used to investigate the effect of size on coating in the MAIC system. The

percentage of surface coverage achieved for each size is shown in Fig. 22. The largest magnets with a mean size of 2.7 mm gave the best surface coverage results. This is probably due to the fact that larger particles have more inertia, higher kinetic energy and higher rotational speeds, and hence are better able to break up guest particle agglomerates due to larger impaction forces on collision.

The motion of the magnetic particles was also examined using a high-speed digital camera. This was done to study the effect of the motion of the magnetic particles on the quality of the surface coverage obtained. A small experimental system consisting of magnets, host and guest particles was assembled similar to that used for the parameter studies. Using the camera, the movement of the magnetic particles was observed at different frequencies at a fixed current of 5 A. The first important observation made was that in addition to the magnetic particle moving haphazardly in all directions (translation), they were also spinning furiously (rotation). The movement of the magnetic particles at different frequencies was measured and recorded. These recorded images were further analyzed to obtain approximate values for the translational and rotational motions. The translational and rotational speeds as a func-
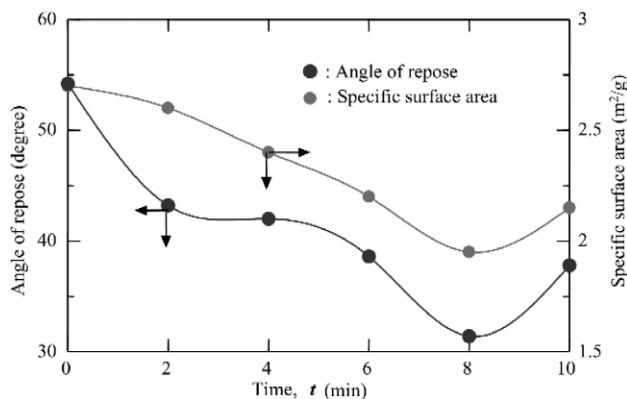


Fig. 18. Flowability and specific surface area as a function of time for cellulose coated with silica in the theta composer.
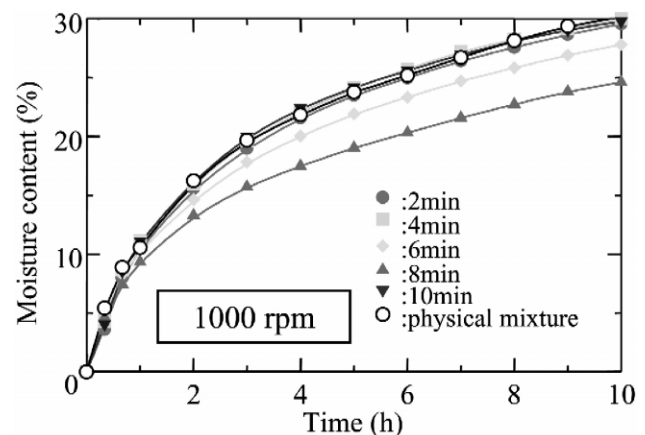


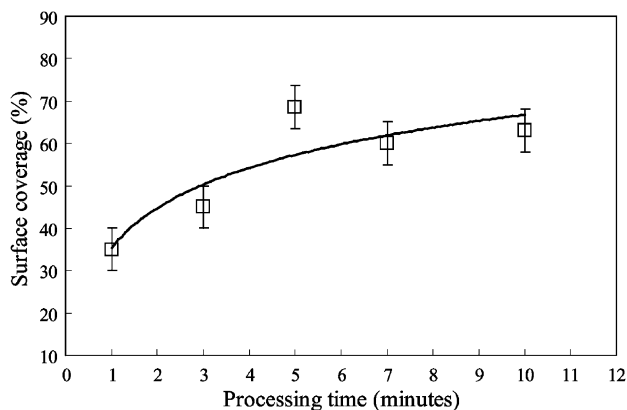Fig. 19. Moisture absorption as a function of time for cellulose processed in the theta composer.

Fig. 20. Surface coverage as a function of processing time (PMMA/ Al$_2$O$_3$).

Fig. 22. Surface coverage of coated products as a function of magnetic particle size.

tion of frequency were then related to the previous study of surface coverage as a function of frequency. Thus, the relationships of the surface coverage as a function of translational and rotational speed were obtained (Figs. 23 and 24). The second important observation (obtained from the figures) showed that the effect of rotational speed of the magnetic particles is much more significant than translational speed on the coating process. In fact, Fig. 24 indicates that there is no change in the percent of surface coating as the translational speed is increased from 36 to 60 cm/s.

The combination of parameter and magnetic particle motion studies suggest that the primary motion due to the magnetic field is the spinning of the magnetic particles, promoting deagglomeration of the guest particles, as well as the spreading and shearing of the guest particles onto the surface of the host particles. However, the effect of the translational speed is also significant as it allows for the impaction of one particle onto another promoting coating. Further studies are clearly needed in this area to clarify these phenomena. A schematic diagram of a proposed mechanism of coating in the MAIC derived from this
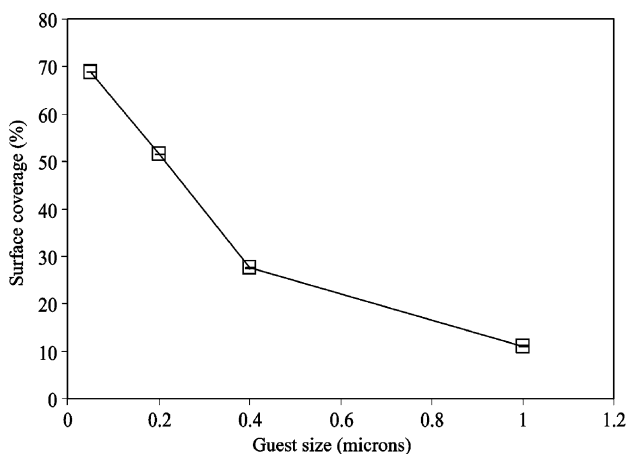
study is shown in Fig. 25. The interactions shown in Fig. 25(b)–(e) are occurring simultaneously to give the coated particle depicted in Fig. 25(f).

### 5.1.3. Surface modification of magnesium

The Nara Hybridization system is able to provide very high shear forces (rotating speed up to 16,000 rpm) to the particles being processed. In addition, the water bath chamber of the system makes it possible to operate at various temperatures. These unique features have been utilized to coat powdered magnesium host particles (75 $\mu$m) with silica (0.7 $\mu$m) and wax (16 $\mu$m) guest particles. Magnesium powder is used in flares and tracer bullets but has a very poor shelf life because it is very hydroscopic and its surface reacts rapidly with water vapor. Therefore, it is desirable to coat magnesium powder with a discrete coating of wax or hydrophobic silica to increase its humidity resistance without sacrificing the firing properties of magnesium. Thus, wet coating processes cannot be used.

The batch size of the magnesium samples used was between 20 and 25 g. The range of rotating speeds and processing times was 5000–12,000 rpm, and 2–4 min, respectively. The temperature of the system used was

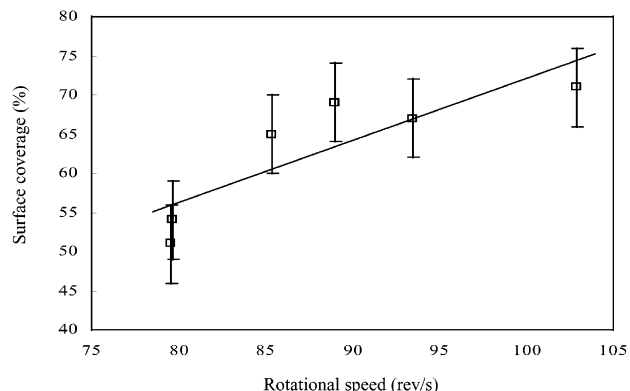Fig. 21. Surface coverage of coated products as a function of guest particle size.

Fig. 23. Surface coverage of the coated products as a function of the rotational speed of the magnetic particles.
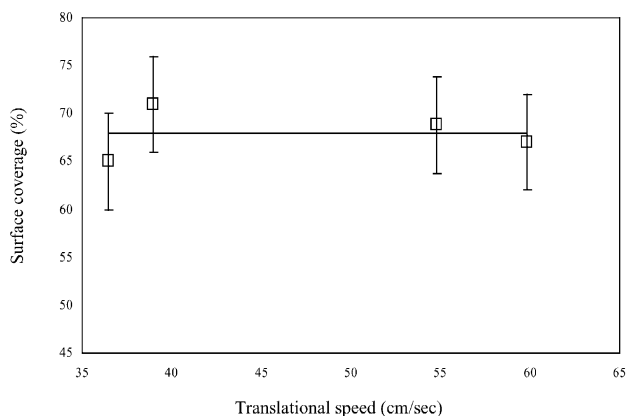
Fig. 24. Surface coverage of the coated products as a function of the translational speed of the magnetic particles.
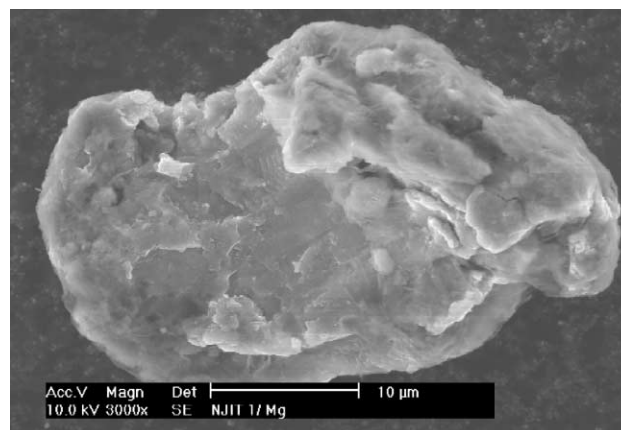


Fig. 26. Surface morphology of unmodified ground magnesium powder.

varied between 22°C and 60°C by varying the temperature of the inlet water into the cooling jacket of the hybridizer. The weight percentage of wax used was 2–4% and that of silica used was 1–2%. The unmodified and modified magnesium samples were characterized by ignition quality, using SEM, reaction testing, humidity testing (with water vapor), and BET surface area measurements.

SEM micrographs of the as-received Mg powder and Mg coated with wax are shown in Figs. 26 and 27. Upon ignition, the coated magnesium powder samples behaved the same as the fresh uncoated magnesium powder samples. Some typical humidity test and reaction test results are shown in Figs. 28 and 29, respectively. These results indicate that using the hybridizer (similar results were obtained using MAIC) to coat wax and silica particles onto magnesium powder can significantly reduce the tendency for magnesium to absorb water from the air. When operat-

ing under various conditions, wax particles are deformed to a different extent, hence producing different surface coverage. The high shear force provided by the hybridizer allowed the silica particles to be evenly distributed over the surface of magnesium particles (even within cracks). The reaction testing showed that the pressure due to released hydrogen gas from the reaction with water vapor decreased significantly as a function of time when silica and wax were coated onto the magnesium particles. BET surface area measurements also indicated a decrease in specific surface area, implying that the deformed wax particles block some of the entrance at surface cracks of the magnesium particles.

### 5.1.4. Deactivated sintering by surface modification

Deactivated sintering, the opposite of activated sintering [90,91], is defined as a process whereby the surface of
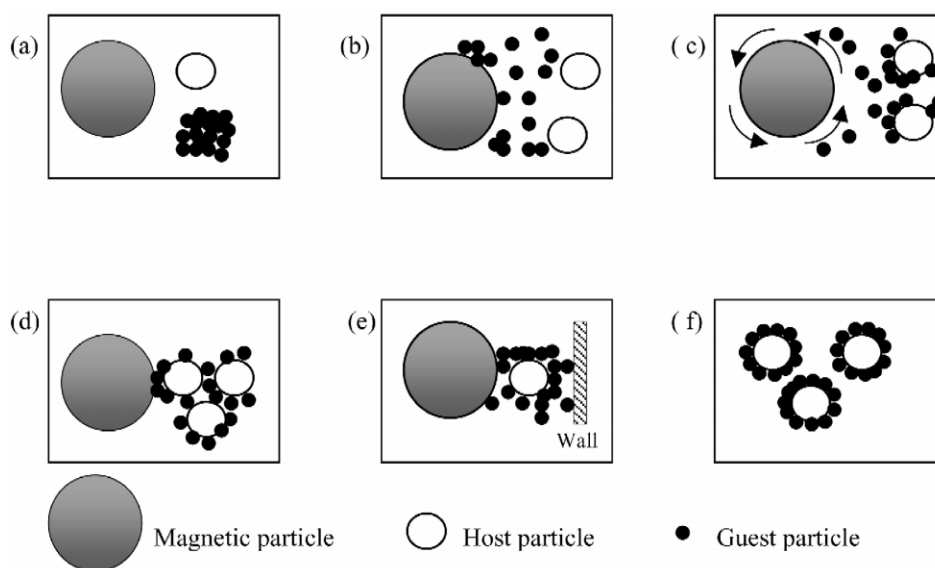


Fig. 25. Mechanism of coating in the MAIC process: (a) excitation of magnetic particle (b) deagglomeration of guest particles (c) shearing and spreading of guest particles on the surfaces of the host particles (d) magnetic–host–host particle interaction (e) magnetic–host–wall interaction, and (f) coated products.

Fig. 27. Surface morphology of magnesium particles coated in the hybridizer for 2 min at 10,000 rpm with 2% wax.



Fig. 29. Reaction testing of uncoated and coated magnesium powder.

particles are coated with another material to delay, and/or reduce the sintering of the materials [92], hence causing an increase in the sintering temperature. MAIC, mechanofusion (MF), and the hybridizer (HB) were used to coat several host particles with small amounts of the highly refractory SiC (guest particles) to promote deactivated sintering [93]. The host particles chosen are either non-porous, glass beads, or porous, a mixture of alumina and silica (cracking catalyst). The properties of these particles and those of SiC are listed in Table 1. The operating parameters for each device are given in Table 2. The results of this study are presented in the following sections.

*5.1.4.1. Glass beads coated with SiC.* Glass beads samples were not processed in the HB since they are brittle and would have been broken by the machine. The samples prepared in the MAIC and MF used two different wt.% of
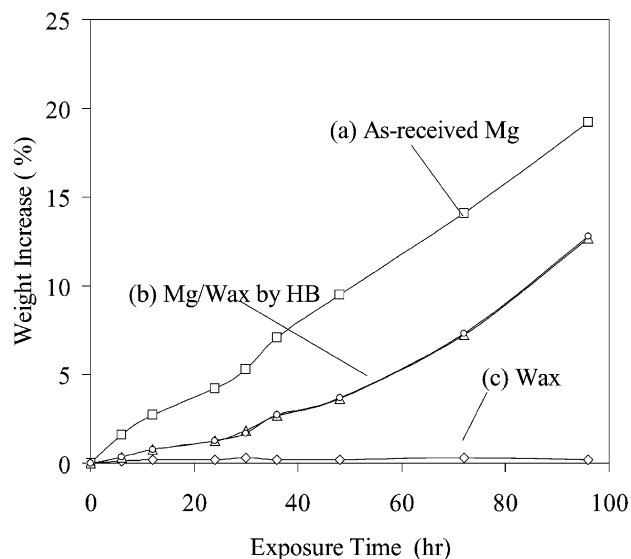
guest particles, 0.8% and 8%. This was done to examine the degree of sintering as a function of guest wt.%. The coated samples, as well as the uncoated glass beads were heated to 600°C, 700°C and 800°C, respectively in a constant rate dilatometer. The dilatometer is used to estimate the minimum sintering temperature of powders as described by previous investigators [94,95]. At 600°C, the uncoated sample showed beginning signs of sintering with some increases in contact area. This increase in contact area was not visible with the 0.8% and 8% guest coated samples processed in MAIC. At 700°C, most of the uncoated sample was fused together, whereas the coated samples remained as individual particles, as shown in Fig. 30(a)–(c). At 800°C, both the uncoated and the 0.8 wt.% coated samples were complete fused, as shown in Fig. 31(a) and (b), respectively. However, the 8 wt.% guest coated sample still remained individual particles with only a small amount of neck growth visible (Fig. 31(c)). This clearly showed that thicker surface coating results in better promotion of deactivated sintering. Similar results were obtained for the MF processed particles.

*5.1.4.2. Alumina–silica catalyst coated with SiC.* The alumina–silica catalytic support was not run in MF due to the



Fig. 28. Hydrothermal testing of (a) as received magnesium, (b) coated magnesium and (c) wax.

Table 1
Properties of host and guest particles

| Samples | Density (g/cm³) | Tm (°C) | Size (μm) | Description |
|---|---|---|---|---|
| Glass beads | 2.5 | 705 | 300 | Spherical, smooth, non-porous |
| Alumina–Silica | 3.6 | ~ 2000 | 50 | Irregular, porous |
| SiC | 3.2 | 2700 | 0.5 | Irregular |

Table 2
Operating parameters for MAIC, mechanofusion and the hybridizer

| Samples | Processing time (min.) | Wt.% guest | Total batch size (g) |
|---|---|---|---|
| *MAIC* | | | |
| Glass beads/SiC | 10 | 0.8, 8 | 10 |
| Alumina/SiC | 2.5, 5, 10 | 2 | 10 |
| *Mechanofusion* | | | |
| Glass beads/SiC | 10 | 0.8, 8 | 100 |
| Alumina/SiC | N/A | N/A | N/A |
| *Hybridizer* | | | |
| Glass beads/SiC | N/A | N/A | N/A |
| Alumina/SiC | 10 | 2 | 50 |

large batch size required to run the device. The mean particle size (based on a volume distribution) of the coated samples from the MAIC and HB, as well as the uncoated sample, is shown in Fig. 32. There was severe size reduction in the HB processed sample and hence the sample was not used in the dilatometry analysis. A large change in the mean particle size or particle size distribution is not desirable since it will not only affect the dilatometry results but can also affect the functionality of the catalytic support material. Further analysis of the MAIC samples showed that the surface coverage of the sample processed for 10 min was about 50%, compared to 11% and 14%, for the samples processed for 2.5 and 5 min, respectively. Though large surface coverage is desirable to help promote deactivated sintering, the coating must be very discrete so as not to reduce the surface area of the catalytic material by clogging the pores. Thus, dilatometry analysis was only conducted on the uncoated support and the samples processed for 2.5 and 5 min. Further studies of the change in surface area ($m^2/g$) of porous materials as a function of surface coverage are presently being conducted.

Both the coated and uncoated samples were heated to 1250°C and 1550°C. The dilatometry results for the samples (uncoated and coated for 2.5 min) heated to 1550°C are shown in Fig. 33. The figure shows that the sintering temperature of the coated sample (approximately, 1320°C) was 140°C higher than the sintering temperature of the uncoated sample (approximately, 1180°C). SEM micro-

graphs of the samples at 1250°C showed an increase in the contact area of the uncoated sample (Fig. 34(a)), whereas the coated sample (Fig. 34b) remained as individual particles, agreeing with the dilatometry results. Of course, it is likely that sintering in the pore structure of the porous material is unaffected by the surface coating of SiC resulting in a decrease in surface area ($m^2/g$) of the catalyst support even though macroscopic sintering has been deactivated.

### 5.1.5. RFBC as a dry particle coating device

The rotating fluidized bed coater (RFBC) was used to coat PMMA host particles (200 μm) with alumina guest particles (0.7 μm) [12]. When the pressure drop of the system is plotted against the airflow velocity at different rotational speeds in the RFBC, the pressure rises to a maximum at the minimum fluidization velocity ($u_{mf}$). After that, it remains constant with increase in air velocity as the bed expands and bubbles are formed. Due to the radial acceleration, the pressure drop increases with an increase in the rotational speed and the minimum fluidization velocity also increases with rotational speed.

For $u/u_{mf}$ less than 2.0 (relatively few bubbles present), there was little carry-over of PMMA particles during processing and almost 100% of the particles remained in the bed. Operation in this fluidization regime allowed the fine alumina particles to be entrapped by the larger PMMA particles and promoted the formation of an ordered mixture and subsequent coating by the impaction of the guest and host particles due to the high shearing forces. However, when the air velocity was greater than $2u_{mf}$, many guest particles were released by bubble breakage, and then carried away from the plenum chamber with the fluidization air. Therefore, the optimum operating air velocity was determined to be $2u_{mf}$.

The performance of the RFBC was analyzed by measuring the adhesion of the guest particles onto the surface of the host particles. This was achieved by plotting the "sticking ratio" as a function of operating time at different rotational speeds in Fig. 35. The sticking ratio is defined as ratio of the mass of guest particles remaining attached to the surface of the host particles, before and after being subjected to an ultrasonic bath for 1 min. Most of the
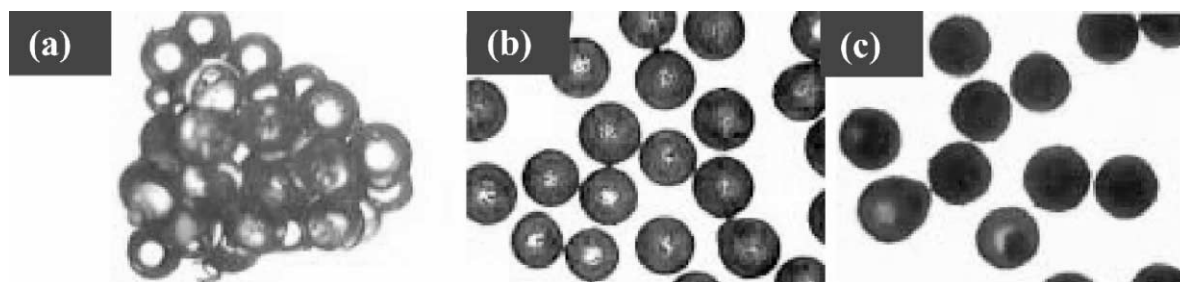


Fig. 30. Optical micrographs showing (a) uncoated samples,(b) samples coated with 0.8 wt.% SiC (MAIC) and (c) samples coat with 8 wt.% SiC (MAIC), run to 700°C in the dilatometer.
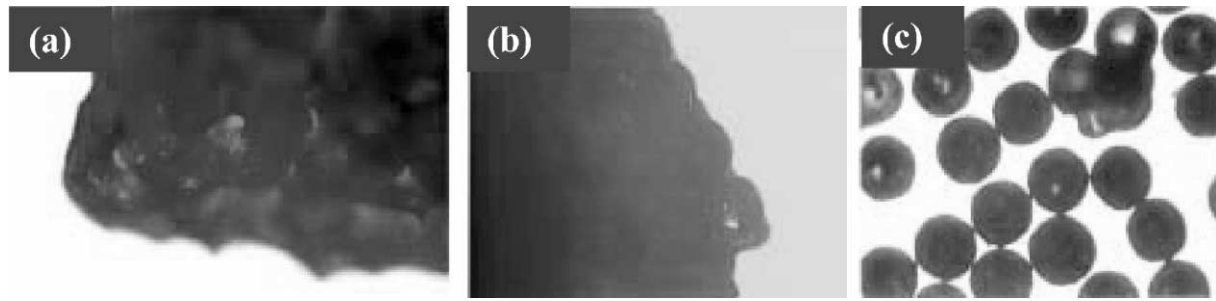
Fig. 31. Optical micrographs showing (a) uncoated samples, (b) samples coated with 0.8 wt.% SiC (MAIC) and (c) samples coat with 8 wt.% SiC (MAIC), run to 800°C in the dilatometer.

alumina guest particles were washed away by the ultra-sonic vibrations at low rotational speeds. Larger sticking ratios were obtained for products processed at high rotational speeds.

Surface morphology (SEM) and elemental mapping (EDX) measurements of the surface of the coated particles were also performed to investigate the changes in surface coverage as a function of processing time. The EDX mapping of alumina for three processing times of 20, 40 and 60 min at $N = 20$ s$^{-1}$ and $u/u_{mf} = 2$ are shown in Fig. 36(a)–(c). These images confirm that larger and more uniform surface coating of PMMA with alumina was achieved with increases in processing time. In fact, a fairly uniform coating of alumina on PMMA is obtained after 60 min. The results above lend support to the feasibility of using the RFBC as a dry particle coating device.

### 5.2. Modeling studies of dry coating

Our long-term objective is to understand the mechanisms of dry coating in all of the machines available so that the effect of various operating variables can be predicted and the processes can be optimized and scaled up. As mentioned in Section 2, some efforts have already been

made to model dry coating processes including mechanofusion [41,66], the hybridizer [43,44,51,67], and MAIC [61]. However, these models are mostly based on phenomenological arguments, and are inadequate for a full understanding of the coating process. Our current efforts include modeling of both the MAIC and MF process. In the long term, we plan to analyze the principal motions/stresses that occur within the process and how they affect the break-up of agglomerates of the guest particles and the subsequent coating of the host particles.

The various dry coating processes are difficult to model because dynamics at several different length and time scales, that differ by several orders of magnitudes, are important. The largest length scale is the device scale, while the smallest length scale is the molecular scale. Only by considering the molecular scale, can one truly understand particle adhesion and the bonding between the guest and host particles. The intermediate scales are those of the host and guest particles. Since the sizes of host, guest and the device differ substantially, the problem of modeling needs to be broken up into a set of simpler problems. Initially, we are addressing the interaction between the device and the host particles. For this purpose, we utilize direct numerical simulations of specific components of each process. These simulations are described in more detail below.

In the past 2 decades, the mathematical models for inelastic particle collisions, their numerical solution, and
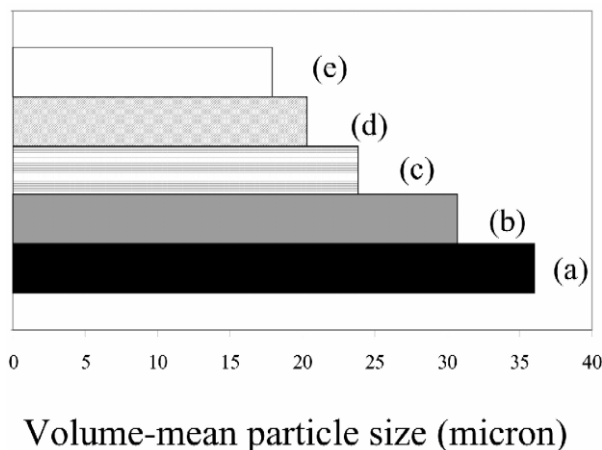


Fig. 32. Volume-mean particle size of (a) uncoated catalytic support, (b) 2.5-min MAIC, (c) 5-min MAIC, (d) 10-min MAIC and (e) 2-min HB processed sample.
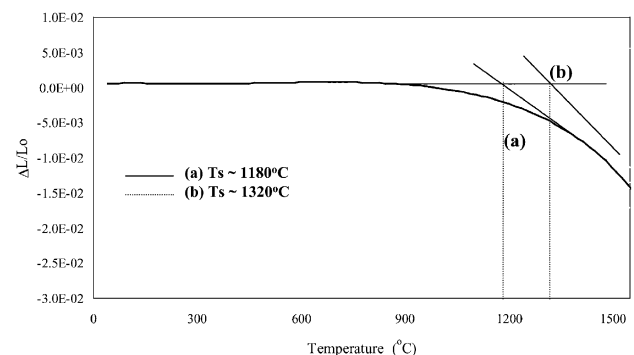


Fig. 33. Elongation vs. temperature for (a) uncoated sample and (b) 2.5 min coated MAIC sample, run in the dilatometer to 1550°C.
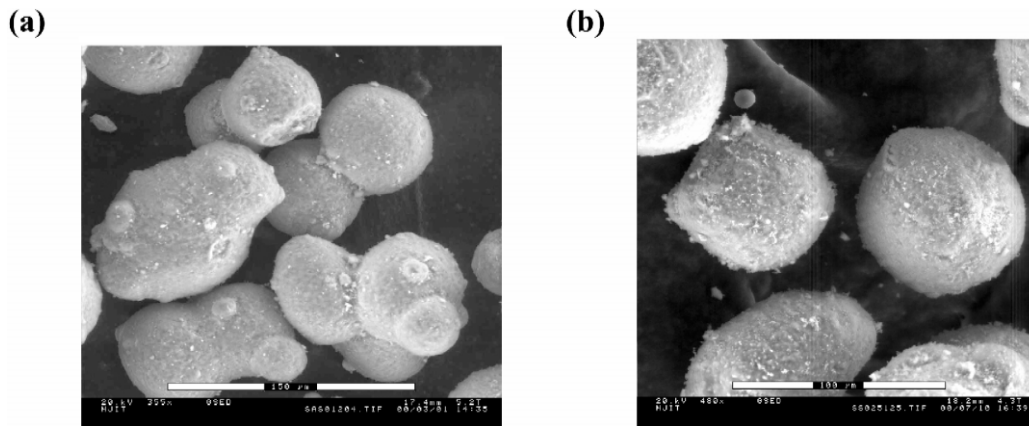
Fig. 34. SEM micrographs for (a) uncoated samples and (b) 2.5-min coated MAIC sample, run in the dilatometer to 1250°C.

the available computational power have all improved considerably. That has made direct numerical simulation, for example, discrete element modeling (DEM), of particulate flow processes possible for a wide range of applications [96–108]. These models use particle–particle interactions ranging from frictionless, elastic, hard sphere formulations to elastic-plastic soft particle interactions including friction with a large, but finite, number of elements. Ideally, one could carry out direct numerical simulation for any coating process. However, in modeling these processes where the particles (guest and host) vary by at least an order of magnitude in size, the usual DEM techniques are not feasible due to the need for including too many particles in the simulation. Therefore, novel schemes are required. The initial approach involves looking at the particle interactions at different length scales, and integrating the results into a simplified device level simulation.

A number of different models of particle–particle interactions [109–114] exist in the literature including normal compliance in loading and unloading, tangential compliance under various normal load conditions, and friction. Based on the Hertz–Mindlin [115] type approach, Walton [105,106,116] and Thornton [117,118] propose normal compliance models taking into account elastic and elastic-
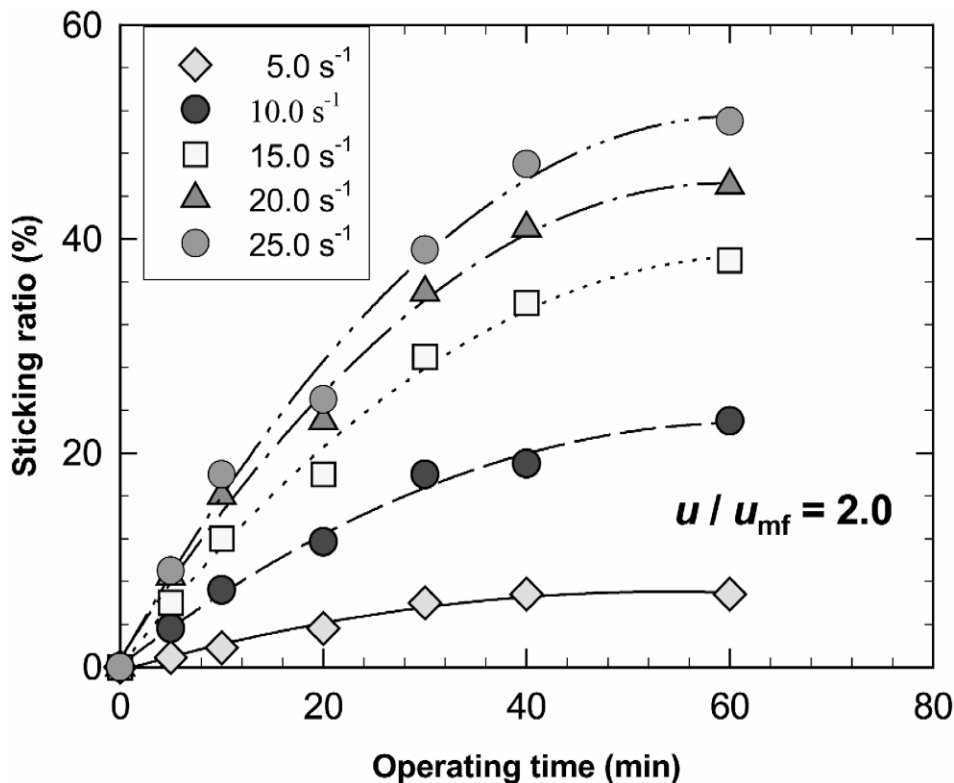


Fig. 35. Sticking ratio as a function of operating time at different rotational speeds.
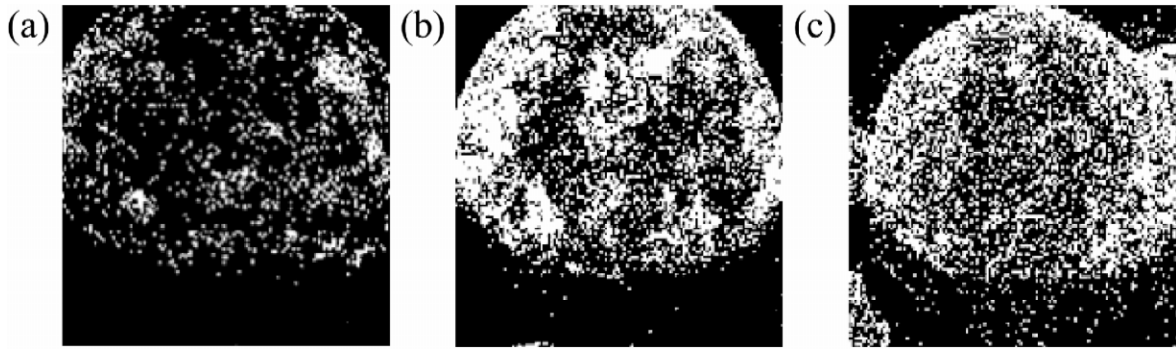
Fig. 36. EDX mapping of alumina on the surface of PMMA at different processing times of (a) 20 min, (b) 40 min and (c) 60 min ($N = 20$ s$^{-1}$, $u/u_{\mathrm{mf}} = 2.0$).

plastic deformations. Walton [116] also utilized a simplified version of the Mindlin–Deresiewicz [119] tangential compliance model that takes into account the loading history. We use this approach in our DEM simulations, and the reader is referred to Refs. [105,106,116] for details. For normal force, we adopt a partially latching-spring. In this model, during loading a linear spring with the spring constant $K_1$ is used, while a stiffer linear spring is used during the unloading (restoration) stage, with spring constant $K_2$. The coefficient $K_2$ can be decided from the given coefficient of restitution $e$, assumed to be independent of the impact velocity, which is defined as

$$e = \sqrt{\frac{K_1}{K_2}} \tag{1}$$

The normal forces during loading, $N_1$, and during unloading, $N_{\mathrm{u}}$, are given by

$$\begin{cases} N_1 = K_1 \cdot \alpha & \text{for loading} \\ N_{\mathrm{u}} = K_2 \cdot (\alpha - \alpha_0) & \text{for unloading} \end{cases} \tag{2}$$

where $\alpha$ is the relative approach (overlap) after initial contact, and $\alpha_0$ is the finite plastic deformation.

The tangential force model used is also according to Walton. The effective tangential stiffness, $K_{\mathrm{T}}$ is a function of normal stress, and is given by

$$K_{\mathrm{T}} = \begin{cases} K_0 \left( 1 - \dfrac{T - T^*}{\mu N - T^*} \right)^{\gamma} & \text{for slip in one direction} (T \text{ increases}) \\ K_0 \left( 1 - \dfrac{T - T^*}{\mu N + T^*} \right)^{\gamma} & \text{for slip in another direction} (T \text{ decreases}) \end{cases} \tag{3}$$

where $T$ is the total tangential force; $K_0$ is the initial tangential stiffness; $\mu$ is the coefficient of friction; $N$ is the total normal force; $\gamma$ is a fixed parameter usually set to one third; $T^*$ is the loading reversal value, which is initially zero, is subsequently set to the value of the total tangential force, $T$, whenever the relative tangential slip reverses direction. It is scaled in proportion to any change

in the normal force from the previous time step. The new tangential force $T'$ is given by the expression,

$$T' = T + K_{\mathrm{T}} \Delta S \tag{4}$$

where $\Delta S$ is the amount of relative surface displacement between the contact particles.

### 5.2.1. Modeling of the MAIC process

Our modeling efforts have been complemented by detailed experimental observations. For example, previous modeling for MAIC assumed that the principal action is the high-speed translations and collisions of magnetic particles leading to energetic collisions between the host and guest particles [61]. However, our careful experimental observations showed that this is not the case. First, we systematically evaluated the time evolution of coating in MAIC, by examining a series of SEM images at increasing processing times. These images show that for very short processing time, the host particles are covered by discrete clumps of guest particles, indicating that the guest particles are initially agglomerated and collisions between individual guest particles or between individual guest and host particles do not take place. For longer processing time, however, an even coating of the guest particles can be observed. Thus, the essential process in MAIC is simultaneous de-agglomeration, guest particle rearrangement and coating.

Another important experimental observation that we made concerned the individual motion of the magnetic particles. While not noticeable by the naked eye, observations using a high-speed video show that the principal motion is rotation (spin) and not translation. In fact, the coating coverage for our model system (PMMA + alumina) correlates with the measured level of spin and not the level of translation as was proposed in Ref. [61]. Therefore, it is necessary to carry out modeling and computer simulations of MAIC process to gain a better understanding of the nature of the particle motion caused by the fluidization and to verify the experimental observations described above.

For DEM simulations, in addition to the usual mechanical forces, we need to incorporate the magnetic force and torque. For that purpose, each magnetic particle is treated as a small magnetic dipole for the sake of simplicity. When the particles are subjected to an external oscillating magnetic field the amount of actual magnetization will change, and there will be a hysteresis effect. However, for the sake of simplicity it is assumed that these particles have a constant magnetic dipole moment. Then the torque, $\mathbf{T}_{ext}$, existing on a magnetic particle due to the external field is given by:

$$\mathbf{T}_{ext} = \mathbf{m} \times \mathbf{B}_{external} \tag{5}$$

where $\mathbf{m}$ is the magnetic dipole moment of the particle and $\mathbf{B}_{external}$ is the magnetic flux density of the external field. While the exact expressions for the magnetic flux density in a finite-sized field coil are complex, our first assumption is to consider the coil as an infinite length solenoid. Thus, $\mathbf{B}_{external}$ is given by:

$$\mathbf{B}_{external} = \mu_0 N I \hat{\mathbf{k}} \tag{6}$$

where $\mu_0$ is the permeability, $N$ is the number of turns in the coil and $I$ is the current in the coil given by $I = I_0 \sin(\omega t)$, and $\hat{\mathbf{k}}$ is the unit vector in the direction of the solenoid axis. Since the current oscillates at the frequency of $\omega$, the external field also oscillates at the same frequency. Thus, the torque, Eq. (5), acting on the particle is time varying. If the torque were constant, then the magnetic particle will tend to align itself with the flux and in the presence of any damping effects, it will eventually come to rest. However, since the flux is time-variant, its direction continuously switches, and the magnetic particle cannot come to rest under small damping. As a result, the applied torque would cause the particle to spin.

Apart from the effect of the external field, the particles themselves generate a magnetic field and that field varies strongly with spatial position. This dipole–dipole induced flux density, $\mathbf{B}_{dipole}$ is given by:

$$\mathbf{B}_{dipole} = \frac{\mu_0}{4 r^5 \pi} \left[ 3(\mathbf{m} \cdot \mathbf{r})\mathbf{r} - r^2 \mathbf{m} \right] \tag{7}$$

where the vector $\mathbf{r}$ is the position where the field is computed with respect to the dipole coordinate system and $\mathbf{m}$ is the magnetic dipole moment. Due to this field, in addition to generating a net torque, there is also a net magnetic force on the particle and the particle is subjected to translation in addition to rotation. The net force, $\mathbf{F}$, acting on a magnetic particle due to the combined magnetic flux, $\mathbf{B}$, is:

$$\mathbf{F} = (\mathbf{m} \cdot \nabla)\mathbf{B} \tag{8}$$

and the net torque, $\mathbf{T}$, on a particle is:

$$\mathbf{T} = \mathbf{m} \times \mathbf{B} \tag{9}$$

where $\mathbf{B}$ is the total magnetic flux density which includes the external field. In case of an infinite solenoid and a single magnetic particle, the magnetic flux density is uniform in space, hence there is no net magnetic force on the particle and there is only a net torque given by Eq. (5). Thus, a simple equation for the rotational motion of a spherical particle is:

$$\mathbf{J}\ddot{\boldsymbol{\theta}} = \mathbf{m} \times \mathbf{B} \tag{10}$$

While not clear in the above form, Eq. (10) is highly non-linear. We note that in a real situation the magnetic flux density due to an external coil is not uniform, hence the particle is subjected to an additional magnetic force. From the equations above, it is evident that the combined
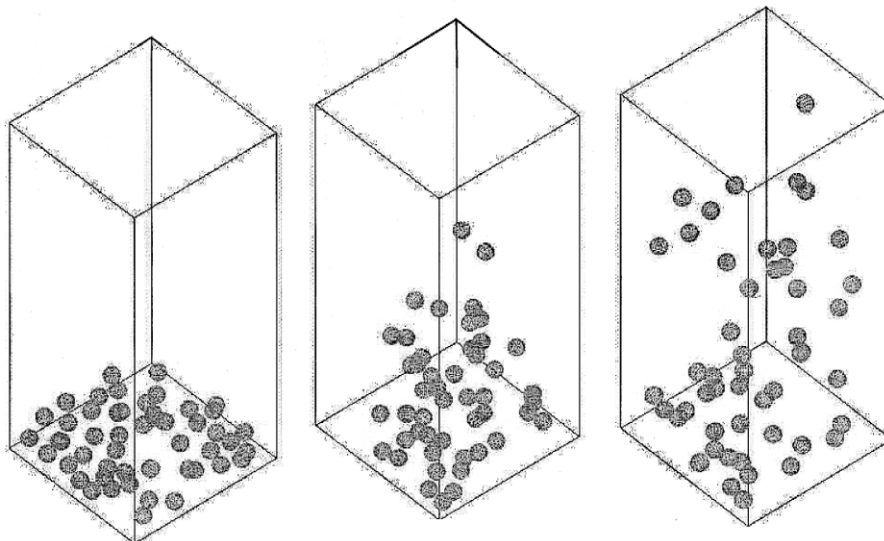


Fig. 37. Fluidization of 50 magnetic particles as the magnetic field is applied. Left, particles deposited at bottom due to gravity, middle, 0.3 s after the field is applied, right, 0.9 s after the field is applied.
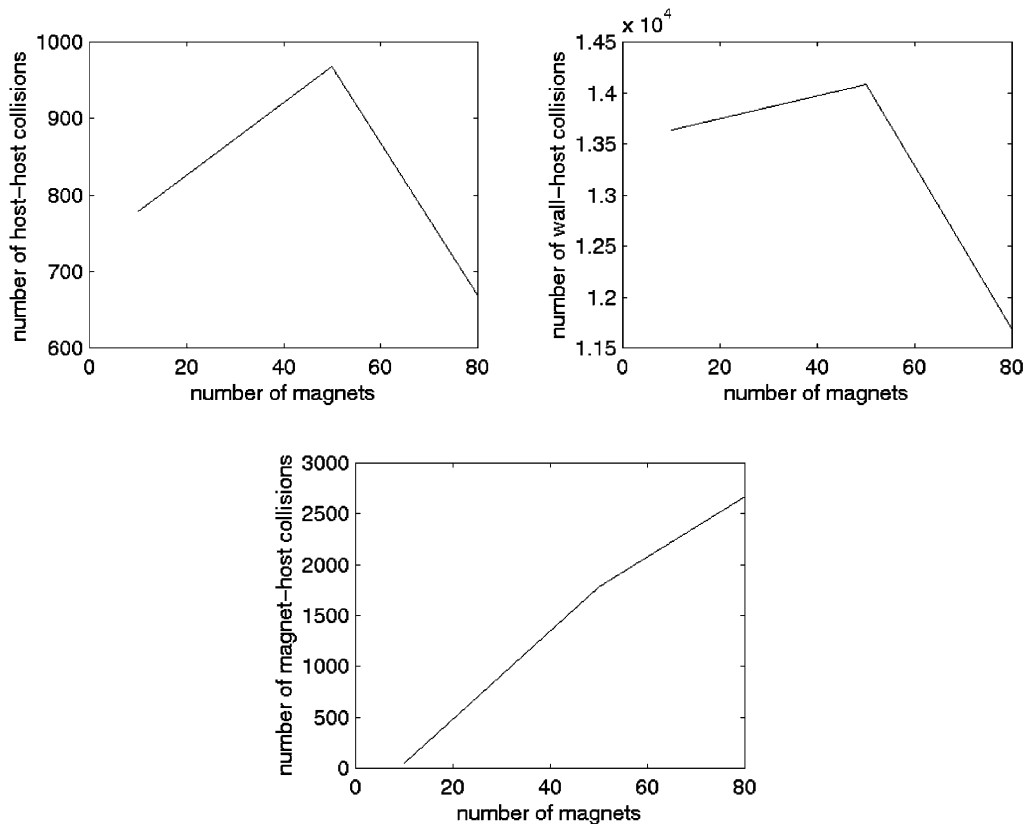
Fig. 38. Simulation results in MAIC for the variation of number of collisions with the number of magnets in the system.

effect of all magnetic interactions could make the particles spin, translate, and collide with the walls of the container and other particles. These collisions eventually fluidize the whole system of magnetic particles. When the other particles (non-magnetic, e.g., host particles to be coated) are present along with the magnetic particles, the spinning and translation results in the development of local micro-shear causing de-agglomeration of guest particles and coating.

We have carried out extensive simulations of the MAIC system; the results are described in detail in Ref. [69]. Due to the intense computing requirement of DEM simulations, it was not possible to simulate the entire MAIC system containing magnets, hosts, and guests since the total number of particles required to simulate a realistic system (because of the large difference in their sizes) are too many for current available computers. Therefore, our simulations involve either only magnets, or magnets and a limited number of host particles. A typical simulation run for a system of 50 magnetic particles, in a rectangular cell of $2.5 \times 2.5 \times 6.0$ cm is shown in Fig. 37. In this figure, in the left panel, the magnets are deposited at the bottom due to gravity. Upon application of the magnetic field, the magnets get fluidized, and two snapshots, at 0.3 and 0.9 s, are shown in middle and right panels, respectively. From these simulations, various diagnostic quantities can be computed. These include the degree of fluidization, particle velocities (translation and rotation), frequency of colli-

sions between magnets–magnets, hosts–magnets, magnets–walls and host–walls, and maximum normal forces during collisions between host and host. These results can be used in conjunction with statistical modeling to determine processing time, coverage and quality of coatings.

One example of collision results obtained from the simulations is shown in Fig. 38, where the variation in the number of collisions is plotted as a function of magnet loading for a system of PMMA and magnetic particles. Here, the number of collisions is an average per host particle. The simulation is carried out in a rectangular cell
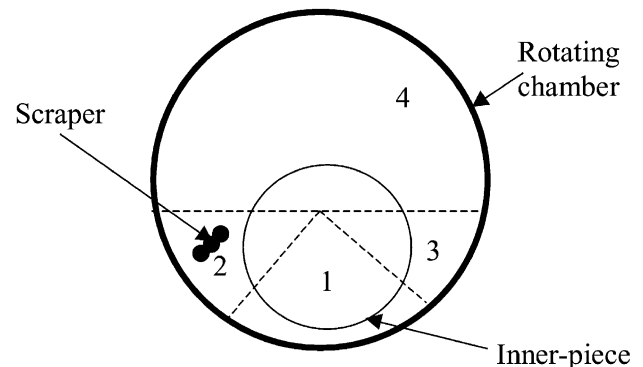


Fig. 39. Simplified geometric model of mechanofusion system for DEM simulation, four zones are defined for diagnostic calculation: (1) inner-piece zone, (2) scraper zone, (3) input zone, (4) free-diffusion zone.

of 2.5 × 2.5 × 6 cm, with 1000 PMMA particles 200 μm in size, and 10–80 magnets of 2.36 mm in diameter.

Fig. 38 shows that initially the number of collisions increases with the number of magnets present for all three cases, i.e., host–host, wall–host and magnet–host. As the number of magnets increase to more than 50, they become disproportionately large as compared with 1000 PMMA particles and the number of host–host and wall–host collisions start to decrease. However, the magnet–host collisions keep increasing with the number of magnets, as expected. Therefore, the total number of collisions that a single host particle will undergo decreases as the number of magnets is increased to 80. This indicates that beyond a certain point, adding more magnets will not help. In this particular case (with 80 magnets), the ratio of the number of hosts to magnets is only 12.5. It should be noted that in a real system, there would be millions of host particles and the ratio of the number of host particles to magnets would never be that low.

We have also conducted scale-up studies of MAIC. The initial results indicate that if the number of magnets per unit volume is preserved, the device can be easily scaled
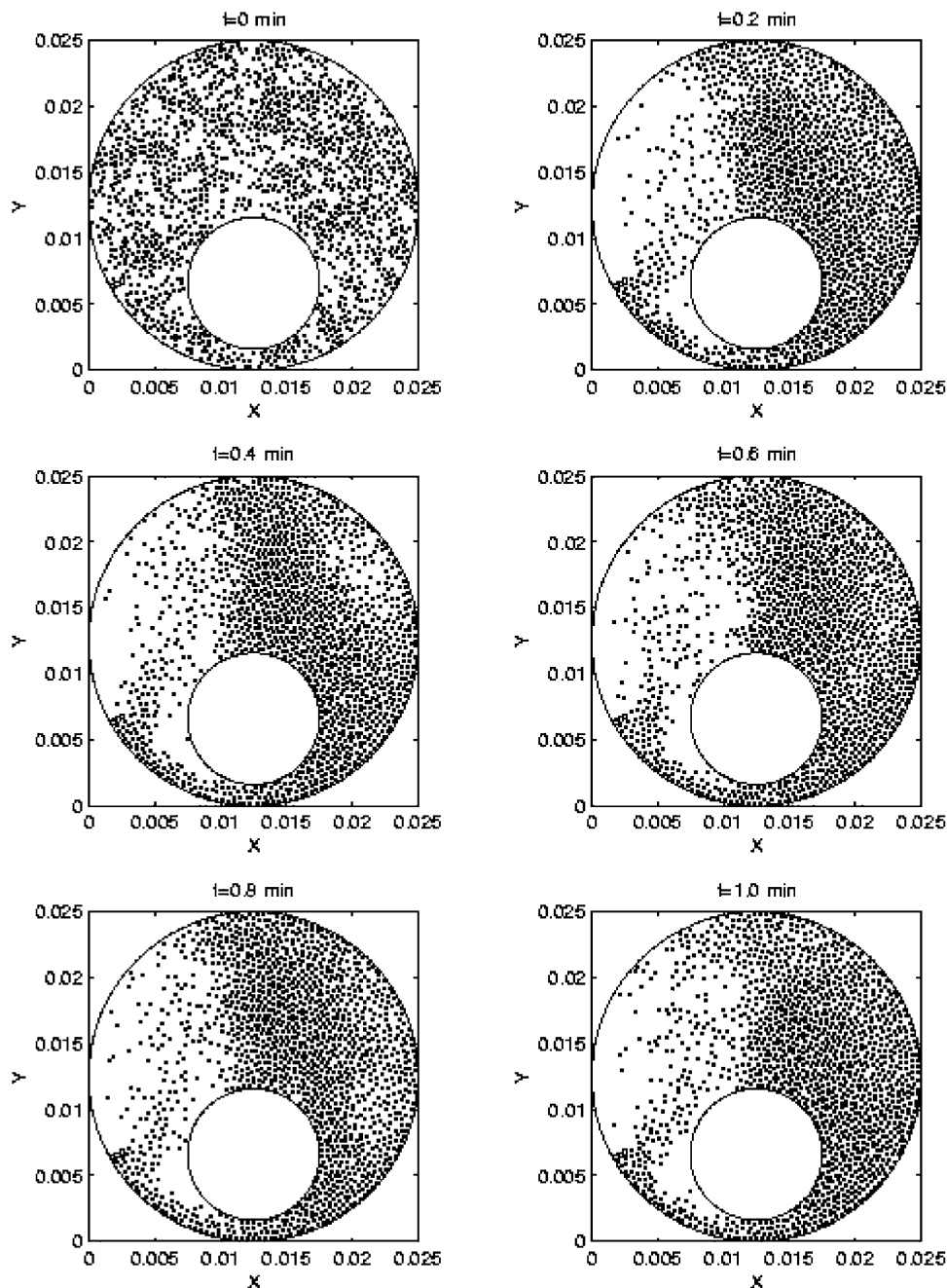


Fig. 40. Evolution of particle configuration for MF system with the scraper.

up by simply applying the same level of magnetic field intensity in a scaled-up device as in a lab scale unit.

### 5.2.2. Modeling of mechanofusion

In modeling of mechanofusion our main objective is to understand the nature of inter-particle forces generated due to the action of the inner piece and the scraper as the rotating chamber is spinning at various speeds. As mentioned before, simultaneous modeling of the guest and the host particles is not feasible due to the large difference in their sizes. Hence, the simulation is done only for the host particles.

The mechanofusion device is modeled as shown in Fig. 39, and is essentially two-dimensional. Since the interaction models are easier to handle between spherical (circular in the two-dimensional case) surfaces, the inner piece is modeled as a cylinder, which is off-center, and the scraper is modeled to be composed of a number of round particles. These simplifications make the simulation easier to carry out without significantly affecting the basic motions. The outer cylinder is allowed to rotate at the desired speed. As a function of the operating parameters, average values of the normal and shear stresses on the particles, particle coordination numbers, velocities, total loading ex-
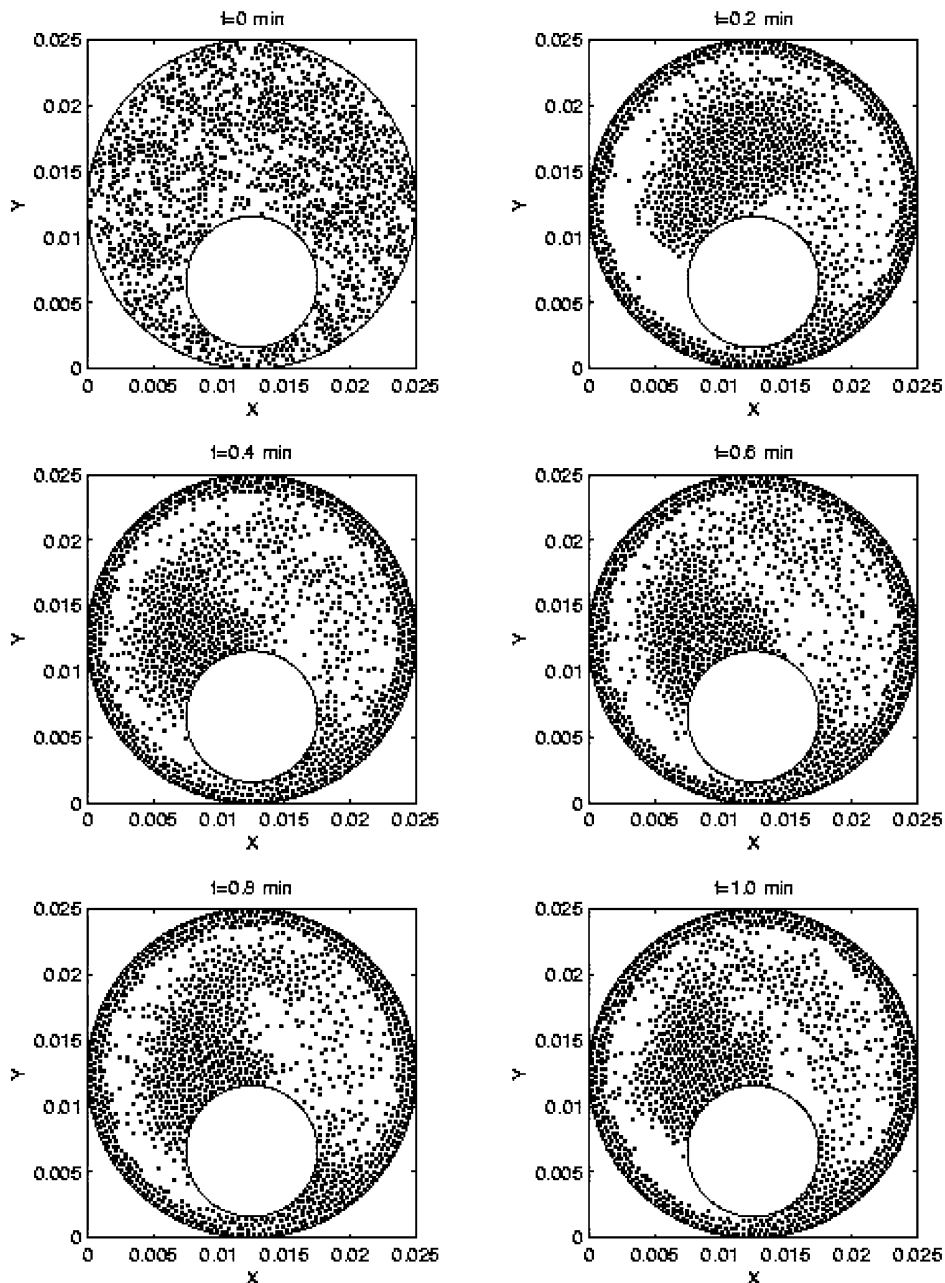


Fig. 41. Evolution of particle configuration for MF system without the scraper.

perienced by the inner piece and other items of interest are computed in various zones within the container. Some of these results are compared qualitatively with force measurements done by Yokoyama et al. [4]. In the long run, these measurements will enable us to determine the effect of various operating parameters, and to determine what levels of normal and shear stresses could affect the de-agglomeration and subsequent coating of the guest particles.

Our preliminary results indicate that the mechanofusion system indeed produces very large normal and shear forces on the particles. In addition, we have studied the system with and without the scraper and found that the presence of the scraper significantly enhances the number and intensity of particle collisions, and thus produces better coating quality, see for example, a series of snapshots in Figs. 40 and 41, where the particle configurations are shown with
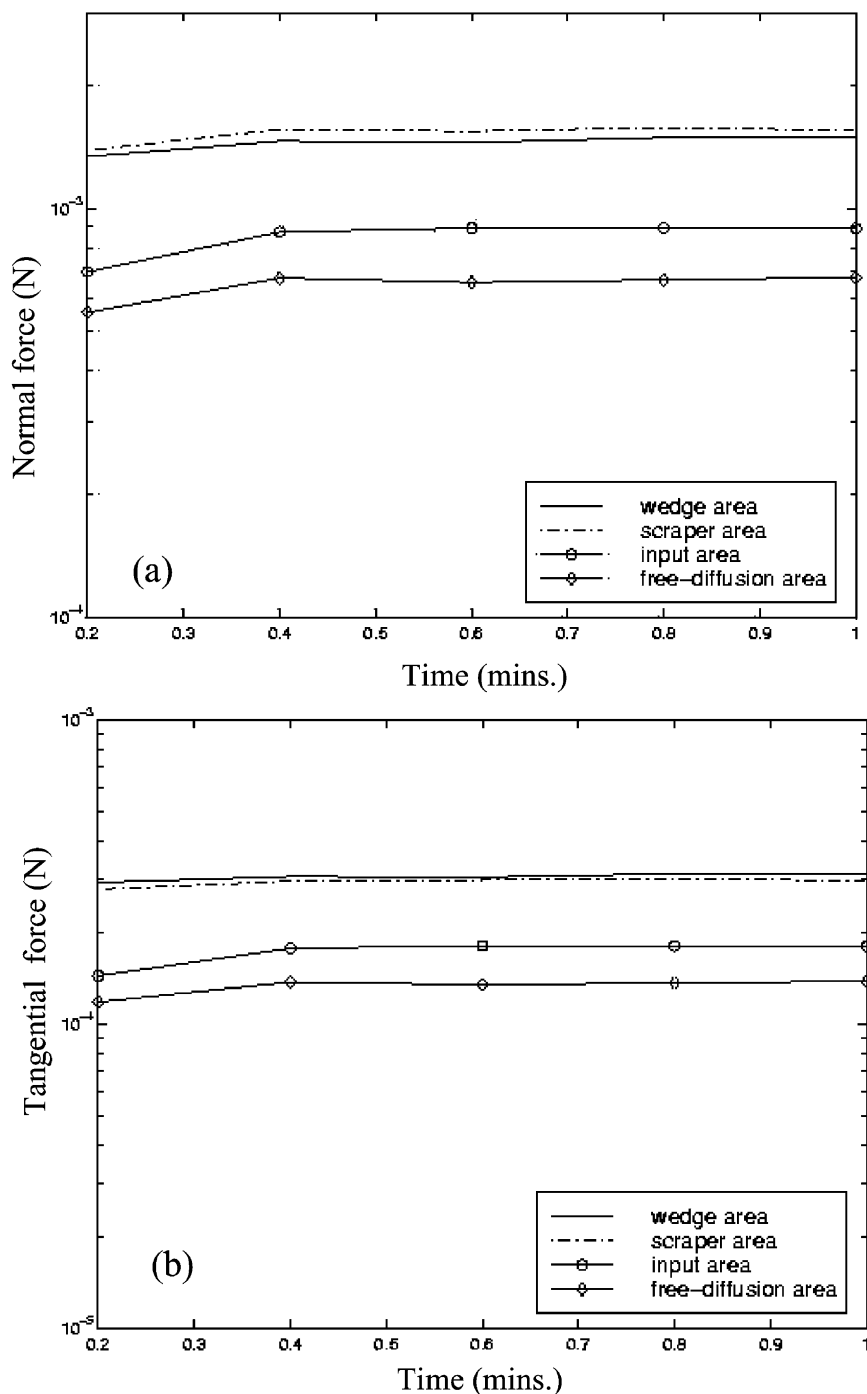


Fig. 42. (a) Average normal force and (b) average tangential force experienced by the particles inside different zones as defined in Fig. 39.

and without the scraper, respectively. As can be seen in the figures, with the scraper present, the particles are removed off the wall and are scattered into free space. However, without the scraper, most particles pack against the outer cylindrical wall of the drum. Hence, it is important to understand the impact of the scraper.

The simulations also give rise to diagnostic quantities such as particle velocities, normal and shear forces during collisions and collision frequencies. An example of the results for the collision forces are shown in Fig. 42, where each curve is for a different zone defined in Fig. 39. As seen in Fig. 42, the forces are high for the inner-piece region and the scraper region. These and other results can be combined to statistically evaluate the coating quality and the time of coating in the system.

## 6. Concluding remarks

Many research papers on dry particle coating processes have appeared in the scientific literature during the past decade. Here, a brief literature review has been presented. These papers describe a variety of machines, which can accomplish dry coating in the laboratory but can also process relatively small batches of powders such as required by the pharmaceutical industry. Yet the operating principles of each device are different; hence the type of coating produced and its application are also different. The current state-of-the-art approach is to use a trial and error procedure to determine whether the process works. This approach is clearly inadequate, because it is very time consuming, and does not allow for determining the conditions for obtaining optimal coating quality. However, to date, very little work has been done to develop macroscopic models for these processes because there is a lack of understanding of the underlying physico-chemical principles that govern the coating process and different devices employ different mechanical mechanisms to achieve coating. Such an understanding is necessary to predict the choice of machines and the right combination of process variables needed to produce composite materials with desired tailored properties. It is, therefore, no wonder that industry has not embraced dry coating processes even though they are environmentally benign since they do not require solvents or even water, save energy because they do not require drying and may be more cost effective than the wet processes which are in widespread use.

In addition to our newly initiated efforts, it is hoped that this review will inspire other researchers to systematically study some of these dry coating processes both experimentally and by mathematical modeling. A theoretical predictive capability is necessary not only to determine which of the devices would give the best results in a specific application, but also to scale-up and optimize the operating conditions for obtaining the best possible coated particles. The current trial and error approach implies that the ma-

chines run under non-optimal conditions, which is another reason why they have not become commercially successful. Based on our research, we strongly believe that dry coating is not only a viable alternative to wet coating, but can be used successfully for certain application where wet coating processes are not feasible.

## References

[1] M. Naito, A. Kondo, T. Yokoyama, ISIJ Int. 33 (1993) 915.
[2] K. Tanno, Kona 8 (1990) 74–81.
[3] K. Mizota, S. Fujiwara, M. Senna, Mater. Sci. Eng., B 10 (1991) 139–147.
[4] T. Yokoyama, K. Urayama, M. Naito, M. Kato, Kona 5 (1987) 59.
[5] M. Satoh, M. Alonso, T. Shigemura, K. Miyanami, T. Suzuki, Trans. Inst. Chem. Eng. 68 (1990) 149.
[6] M. Alonso, M. Satoh, K. Miyanami, Powder Technol. 59 (1989) 65.
[7] M. Alonso, M. Satoh, K. Miyanami, Kona 7 (1989) 97.
[8] M. Koishi, H. Honda, T. Ishizaka, T. Matsuno, T. Katano, K. Ono, Chim. Oggi: Int. J. Chem. Biotechnol. 5 (7–8) (1987) 43.
[9] M. Ramlakhan, C.Y. Wu, S. Watano, R.N. Dave, R. Pfeffer, World Congress on Particle Technology, Brighton, UK, July 7–9, 1998.
[10] B. Chaudhuri, P. Singh, R. Pfeffer, R.N. Dave, World Congress on Particle Technology, Brighton, UK, July 7–9, 1998.
[11] M. Ramlakhan, C.Y. Wu, S. Watano, R.N. Dave, R. Pfeffer, Powder Technol. 112 (1–2) (2000) 137–148.
[12] S. Watano, W.C. Dunphy, R.N. Dave, R. Pfeffer, Adv. Technol. Part. Process.: 1998 AIChE Conf. I (1998) 565–598, November.
[13] J. Hersey, Powder Technol. 11 (1975) 41.
[14] J. Hersey, Powder Technol. 10 (1974) 97.
[15] J. Hersey, J. Pharm. Sci. 63 (12) (1974) 1960.
[16] J. Hersey, W.J. Thiel, C.C. Yeung, Powder Technol. 24 (1979) 251.
[17] J. Hersey, J. Pharm. Pharmacol. 33 (1981) 485.
[18] C.C. Yeung, J. Hersey, Powder Technol. 22 (1979) 127.
[19] C.W. Yip, J. Hersey, Powder Technol. 16 (1977) 189.
[20] N.A. Orr, E. Shotton, Chem. Eng. (1973) 12, Jan.
[21] N.A. Orr, in: P.B. Deasy, R.F. Timony (Eds.), Progress in the Quality Control of Medicines, Elsevier/North Holland Biomedical Press, 1974, Chap. 9.
[22] H. Egermann, N.A. Orr, Powder Technol. 36 (1983) 117.
[23] J.N. Staniforth, J.E. Rees, Powder Technol. 30 (1981) 255.
[24] J.N. Staniforth, Powder Technol. 33 (1982) 147.
[25] J.N. Staniforth, J.E. Rees, J. Pharm. Pharmacol. 34 (1982) 69.
[26] J.N. Staniforth, J.E. Rees, J. Pharm. Pharmacol. 34 (1982) 700.

[27] J.N. Staniforth, J.E. Rees, F.K. Lai, J. Hersey, J. Pharm. Pharmacol. 34 (1982) 485.
[28] J.N. Staniforth, Powder Technol. 45 (1985) 73.
[29] N. Shah, Hosokawa Micron Powder Systems: Pharmaceutical Industry Seminar, Summit, New Jersey, May 19–20, 1998.
[30] P. Bannister, N. Harnby, Powder Technol. 36 (1983) 275.
[31] G.G. Enstad, Inst. Chem. Eng. Symp. Ser. 65 (1981) S2/H.
[32] L. Bryan, Y. Rungvejhavuttivitaya, P.J. Stewart, Powder Technol. 22 (1979) 147.
[33] M.J. Crooks, R. Ho, Powder Technol. 14 (1976) 161.
[34] F.S. Lai, J.A. Hersey, Chem. Eng. Sci. 36 (1981) 1133.
[35] P.L. Stephenson, W.J. Thiel, Powder Technol. 25 (1980) 115.
[36] W.J. Thiel, P.L. Stephenson, Powder Technol. 31 (1982) 45.
[37] F.S. Lai, J.A. Hersey, J.N. Staniforth, Powder Technol. 28 (1981).
[38] P. Thanomkiat, P.J. Stewart, P.S. Grover, Powder Technol. 24 (1979) 97.
[39] W.J. Thiel, L.T. Nguyen, P.L. Stephenson, Powder Technol. 34 (1983) 75.
[40] C.W. Yip, J. Hersey, Powder Technol. 16 (1977) 149.
[41] M. Alonso, M. Satoh, K. Miyanami, Powder Technol. 59 (1989) 45.
[42] M. Alonso, M. Satoh, K. Miyanami, Powder Technol. 59 (1989) 217.
[43] M. Alonso, M. Satoh, K. Miyanami, Powder Technol. 62 (1990) 35.
[44] M. Alonso, A Fundamental Study on the Coating of Powders, Doctoral Thesis, University of Osaka Prefecture, Osaka, Japan, 1991.
[45] T. Yokoyama, K. Urayama, Kona 1 (1983) 53.
[46] M. Koishi, J. Soc. Powder Technol., Jpn. 20 (1983) 772.
[47] M. Koishi, T. Ishizaka, T. Nakajima, Appl. Biochem. Biotechnol. 10 (1984) 259.
[48] H. Honda, K. Ono, T. Ishizaka, T. Matsuno, K. Katano, M. Koishi, J. Soc. Powder Technol., Jpn. 24 (9) (1987) 593.
[49] H. Honda, T. Matsuno, M. Koishi, J. Soc. Powder Technol., Jpn. 25 (9) (1988) 597.
[50] H. Honda, T. Matsuno, M. Koishi, J. Soc. Powder Technol., Jpn. 26 (9) (1989) 666.
[51] H. Honda, M. Kimura, T. Matsuno, M. Koishi, Chim. Oggi: Int. J. Chem. Biotechnol. 9 (1991) 21, June.
[52] T. Ishizaka, H. Honda, Y. Kikuchi, T. Katano, M. Koishi, Chem. Pharm. Bull. 36 (1988) 2562–2569.
[53] M. Senna, Mater. Res. Forum (1999) 312–314, 167–172.
[54] M. Senna, Chem. Rev. 23 (2) (1998) 263–284.
[55] M. Senna, Trans Inst. Chem. Eng. 76 (1998) 767–774, Part A.
[56] M. Senna, China–Jpn. Symp. Particul. 5 (1996).
[57] M. Shimizu et al., J. Soc. Powder Technol., Jpn. 31 (9) (1997) 666.
[58] Y. Fukumori, H. Ichikawa, M. Ueda, Proc. World Congress on Particle Technology 3, Brighton, UK, 1998, 1217.
[59] S. Watano, Y. Imada, K. Miyanami, C.Y. Wu, R.N. Dave, R. Pfeffer, J. Chem. Eng., Jpn. 33 (6) (2000) 848–854.
[60] Y. Kawashima, T. Serigano, T. Hino, H. Yamamoto, H. Takeuchi, Int. J. Pharm. 173 (1998) 243–251.
[61] R. Singh, A. Ata, J. Fitz-Gerald, Surf. Modif. Technol. 10th International Proceedings on Surface Modification Technologies, 1997.
[62] A. Ata, Y.I. Rabinovich, R.K. Singh, Mater. Res. Soc. Symp. (1998) 333–338, Materials Research Society.
[63] J. Fitz-Gerald, R.K. Singh, T. Trottier, P.H. Holloway, Appl. Phys. Lett. 72 (1998) 15.
[64] J. Fitz-Gerald, S. Pennycook, H. Gao, R.K. Singh, Nanostruct. Mater. 12 (1999) 1167–1171.
[65] J. Fitz-Gerald, R.K. Singh, H. Gao, J. Mater. Res. 14 (8) (1999) 3281–3291.
[66] J. Chen, H. Herman, C.C. Huang, Kona 15 (1997) 113–120.
[67] H. Honda, M. Kimura, F. Honda, T. Matsuno, M. Koishi, Colloids Surf., A 82 (1994) 117–128.
[68] R. Mei, H. Shang, J.F. Klausner, E. Kallman, Kona 15 (1997) 132–141.
[69] B. Chaudhuri, Simulation and modeling of magnetically assisted impaction coating (MAIC) process for dry particle coating, Doctoral thesis, May 2000.
[70] J. Szepvolgyi, 1999 AIChE Annual Meeting, Dallas, TX, 1999.
[71] W. Hendrickson, J. Abbott, Process for Making Particle-Coated Solid Substrates, U.S. Patent Laid-Open, 1997.
[72] G.H. Qian, I. Bagyi, R. Pfeffer, H. Shaw, J.G. Stevens, AIChE Journal, In Press.
[73] T. Ishizaka, H. Hondo, Y. Kikuchi, K. Ono, T. Katano, M. Koishi, J. Pharm. Pharmacol. 41 (1989) 361–368.
[74] T. Ishizaka, H. Honda, M. Koishi, J. Pharm. Pharmacol. 45 (1993) 770–774.
[75] M. Naito, M. Yoshikawa, Kona 7 (1989) 119.
[76] D. Liu, P.V. Kamat, J. Electrochem. Soc. 142 (3) (1995) March.
[77] P. Lih, D.D.L. Chung, J. Electron. Mater. 24 (7) (1995) .
[78] E.P. Luther, F.E. Lange, D.S. Pearson, J. Am. Ceram. Soc. 78 (8) (1995) 2009–2011.
[79] K.R. Han, C.S. Lim, M.J. Hong, J. Am. Ceram. Soc. 79 (2) (1996) 574–576.
[80] N. Kawashima, K. Soetanto, K. Watanabe, K. Ono, T. Matsuno, Colloids Surf., B 10 (1997) 23–27.
[81] F. Honda, H. Honda, M. Koishi, J. Chromatogr. 609 (1992) 49–59.
[82] M. Naito, M. Yoshikawa, T. Yotsuya, J. Jpn. Soc. Powder Metall. 37 (1990) 131.
[83] M. Naito, A. Kondo, T. Yokoyama, ISIJ Int. 33 (1993) 915.
[84] T. Asano, Y. Tanaka, M. Fukutomi, K. Komori, H. Inoue, M. Maeda, M. Yoshikawa, M. Naito, IEEE Trans. Magn. 28 (1992) 884.
[85] T.E. Furia, CRC Handbook of Food Additives, The Chemical Rubber, Cleveland, OH, 1968.
[86] M.F. Koenig, S.J. Huang, Polym. Degrad. Stab. 45 (1994) 139–144.
[87] N. Kaya, M. Koishi, Kona 6 (1988) 86–97.
[88] S. Watano, Y. Sato, K. Miyanami, Chem. Pharm. Bull. 44 (8) (1996) 1556–1560.
[89] J.F. Liao, M. Senna, Mater. Res. Bull. 30 (4) (1995) 385.
[90] N.M. Huang, Y.J. Park, D.-Y. Yim, D.Y. Yoon, Scr. Mater. 42 (2000) 421–425.
[91] O.N. Kaidash, Ceram. Int. 24 (1998) 157–162.
[92] L.J. Bonis, H.H. Hausner, Fundam. Phenom. Mater. Sci. 1 (1964) 3–25.
[93] M. Ramlakhan, R.N. Dave, R. Pfeffer, Annual Meeting, AIChE Conference, Nov., 2000.
[94] P. Compo, R. Pfeffer, G. Tardos, Powder Technol. 51 (1987) 85–101.
[95] G. Tardos, D.M. Mazzone, R. Pfeffer, Can. J. Chem. Eng. 62 (1984) 884–887.
[96] C.S. Campbell, C.E. Brennen, J. Fluid Mech. 151 (1985) 167–188.
[97] R.N. Dave, A.D. Rosato, K. Bhaswan, Mech. Res. Commun. 22 (1995) 335–342.
[98] A.C. Gallas, H.J. Herrmann, S. Sokolowski, Phys. Rev. Lett. 69 (1992) 1371.
[99] C. Gardiner, D. Schaeffer, SIAM J. Appl. Math. 54 (1994) 1676–1692.
[100] I. Goldhirsch, J. Sci. Comp. 8 (1993) 1–40.
[101] M.A. Hopkins, J.T. Jenkins, M.Y. Louge, Phys. Fluids A 3 (1991) 47–57.
[102] Y. Lan, A.D. Rosato, Phys. Fluids 7 (1995) 1818–1831.
[103] A. D Rosato, H.-K. Kim, Continuum Mech. Thermodyn. 6 (1) (1994) 1–21.
[104] Y. Taguchi, Phys. Rev. Lett. 69 (1992) 1367.
[105] O.R. Walton, R.L. Braun, J. Rheol. 30 (1986) 949–980.
[106] O.R. Walton, in: M.C. Roco (Ed.), Particulate Two-Phase Flow, Butterworth-Heinemann, Boston, 1992, pp. 884–911.
[107] C. Thornton, K.K. Yin, M.J. Adams, J. Phys. D: Appl. Phys. 29 (1996) 424–435.

[108] C.R. Wassgren, C.E. Brennen, M.L. Hunt, J. Appl. Mech. 63 (1996) 712–719.

[109] B.V. Derjaguin, Kolloid-Z. 69 (1934) 155.

[110] K.L. Johnson, K. Kendall, A.D. Roberts, Proc. R. Soc. London, Ser. A 324 (1971) 301.

[111] B.V. Derjaguin, V.M. Muller, P.Y. Toporov, J. Colloid Interface Sci. (1975) 53.

[112] D. Maugis, H.M. Pollock, Acta Metall. 32 (9) (1984) 1323–1334.

[113] L.N. Rogers, J. Reed, J. Phys D: Appl. Phys. 17 (1984) 677.

[114] D.J. Quesnel, D.S. Rimai, L.P. DeMejo, J. Adhes. Sci. Technol. 9 (1995) 1015–1030.

[115] R.D. Mindlin, J. Appl. Mech. 16 (1949) 259–268.

[116] O.R. Walton, Mech. Mater. 16 (1993) 239–247.

[117] C. Thornton, K.K. Yin, Powder Technol. 65 (1991) 153–166.

[118] C. Thornton, J. Appl. Mech. 64 (1997) 383–386.

[119] R.D. Mindlin, H. Deresiewicz, J. Appl. Mech. 20 (1953) 327.